FIG. 2. Generation and analysis of Rpn10a knock-in mice. (A) Schematic representation of the targeting vector and the targeted allele of the Rpn10 gene. Light shaded box, the Rpn10a cDNA fragment corresponding to amino acids 219 to 376 with a polyadenylation signal. Dark shaded box, Rpn10a exon 7 splicing acceptor sequences followed by a stop codon and polyadenylation signal. Triangles, loxP sequences. Open box, probe used for Southern blot analysis. Arrows indicate positions of PCR primers. (B) Southern blot analysis of genomic DNAs extracted from mouse tails.
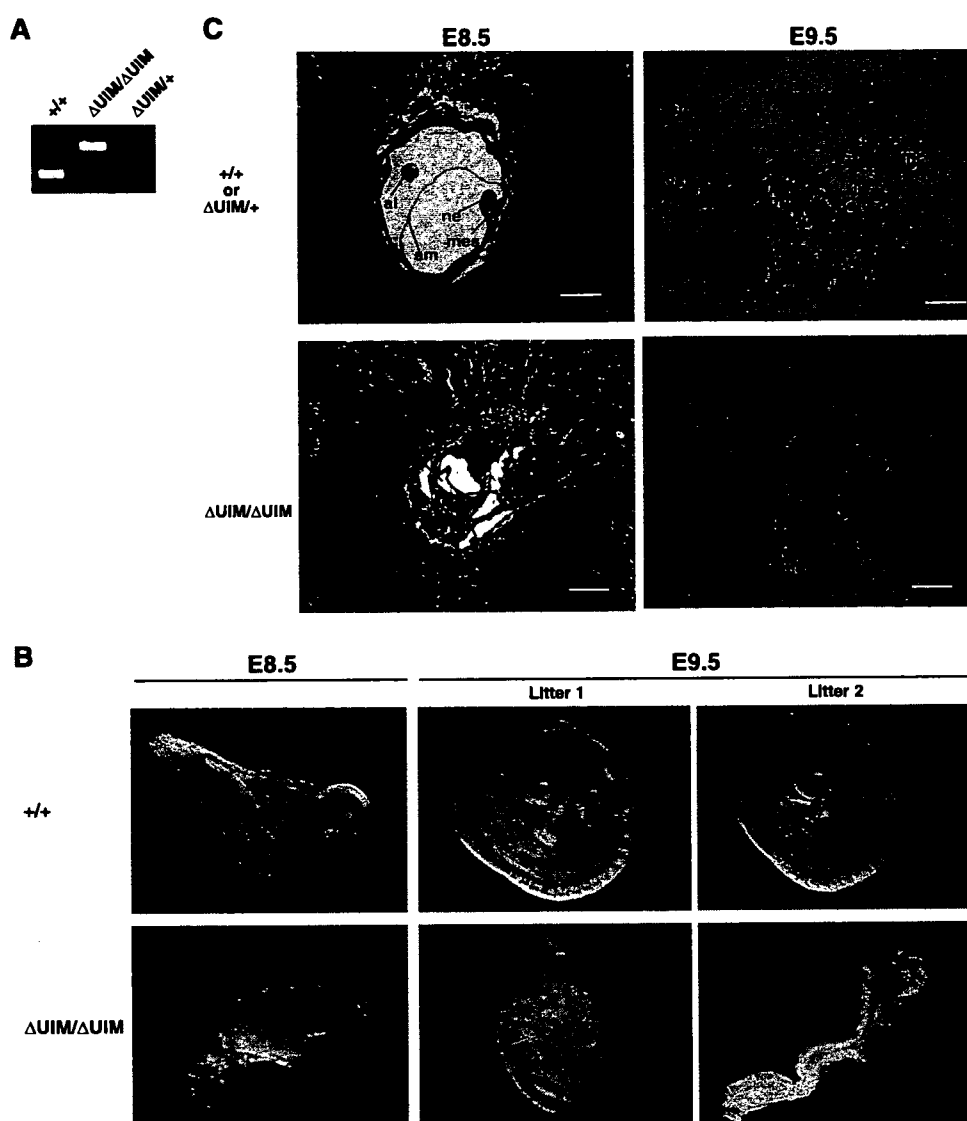
FIG. 3. Developmental arrest of mice deficient in the UIM domains. (A) PCR analysis of genomic DNA extracted from wild-type, Rpn10$^{\Delta UIM/\Delta UIM}$, and Rpn10$^{\Delta UIM/+}$ embryos at E8.5. The amplified fragments derived from wild-type, ΔUIM/+, and ΔUIM/ΔUIM alleles are indicated. (B) Morphology of Rpn10 embryos. Genotypes of embryos were determined by PCR. The longitudinally arranged panels represent littermates. Note the lack of turning of mutant embryos at E9.5. (C) Rpn10$^{+/+}$ (top) and Rpn10$^{\Delta UIM/\Delta UIM}$ (bottom) embryos at E8.5 and E9.5 in utero were sagittally (E8.5) and transversely (E9.5) sectioned and stained with hematoxylin and eosin. Genotypes of embryos were deduced morphologically. Scale bars, 200 μm. ac, amniotic cavity; al, allantois; am, amnion; ch, chorion; en, endocardium; epc, ectoplacental cone; exo, exocoelom; fg, foregut; hf, head fold; hg, hindgut; ht, heart tube; mc, myocardium; mes, mesoderm; ne, neuroectoderm; nf, neural fold; no, notochord; nt, neural tube; vys, visceral yolk sac.

sates. Although the band intensities of proteasome subunits (Rpt6, Rpn1, Rpn2, Rpn6) were comparable between the genotypes, the amount of mHR23B in Rpn10ΔUIM proteasomes was approximately 60% lower than that in Rpn10$^{a/a}$ proteasomes (Fig. 4G), consistent with the previous observations that

the UIM domain of Rpn10 recruits Rad23 species in mammals (7, 17, 25, 46). However, this result also indicates that the UIM domain is not the sole receptor for Rad23 species in mammals, because a portion of mHR23B remained associated with Rpn10ΔUIM proteasomes (Fig. 4G). It should be noted that

Wild-type and mutant alleles are detected as 12.4- and 7-kb bands, respectively. (C) PCR analysis of genomic DNA extracted from the tails of wild-type, Rpn10$^{a/+}$, and Rpn10$^{a/a}$ mice. The amplified fragments derived from wild-type and Rpn10a alleles are indicated. (D) RT-PCR analysis of Rpn10 splice variant transcripts. (E) Liver lysates from 13-week-old mice were immunoblotted with antibodies against the indicated proteins. (F) Lysates from Rpn10$^{+/+}$ and Rpn10$^{a/a}$ livers were fractionated by glycerol gradient centrifugation (10 to 40% glycerol from fraction 1 to fraction 30). (Left) An aliquot of each fraction was used for an assay of chymotryptic activity of proteasomes using succinyl-Leu-Leu-Val-Tyr-7-amino-4-methyl-coumarin (Suc-LLVY-AMC) as a substrate in the absence (top) or presence (bottom) of 0.025% sodium dodecyl sulfate (SDS). (Right) Immunoblot analysis of each fraction was performed using antibodies against the indicated proteins.
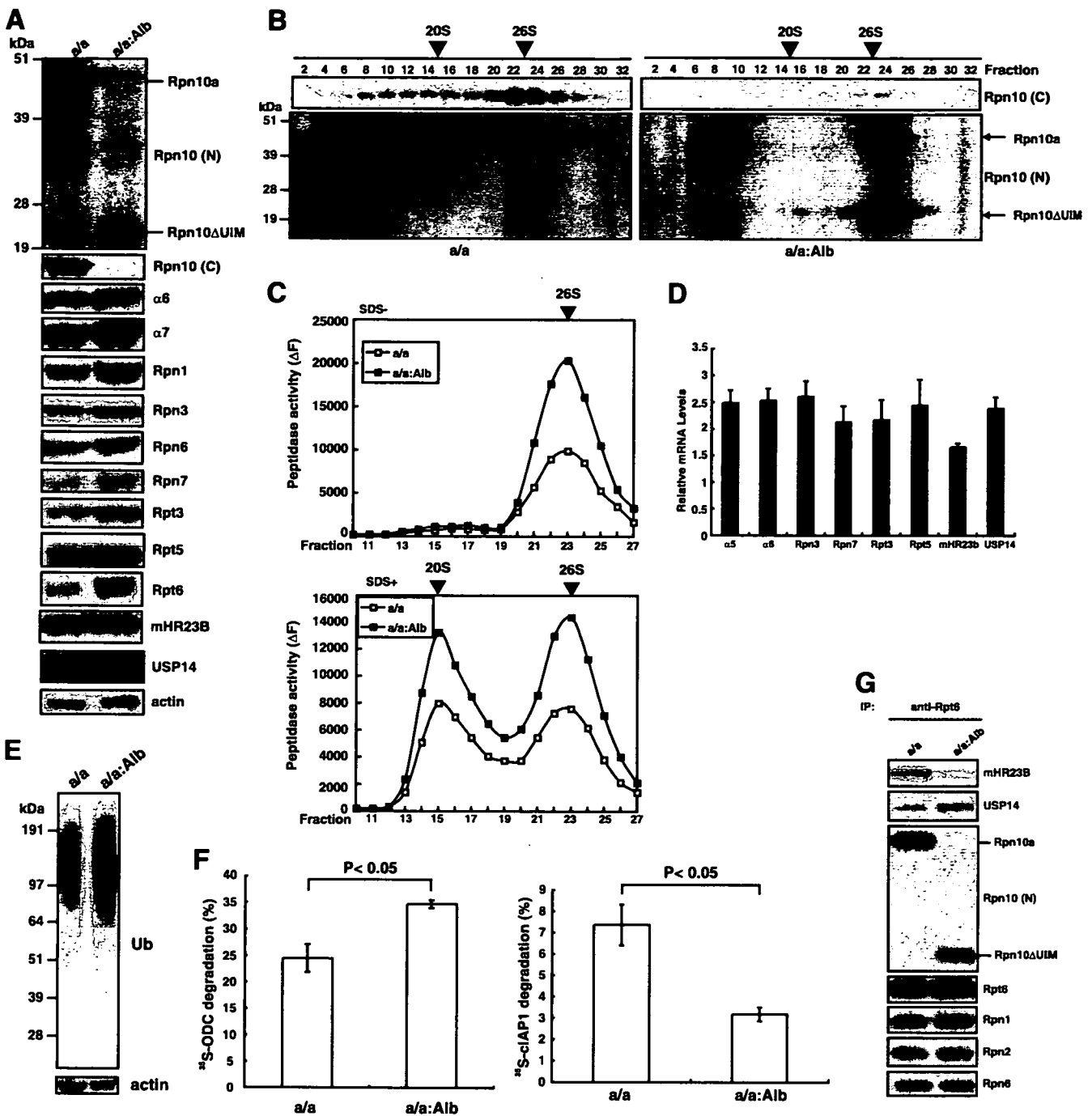
FIG. 4. UIM domain deficiency in the liver causes impaired degradation of ubiquitinated proteins. (A) Homogenates from 6-week-old Rpn10$^{a/a}$ and Rpn10$^{a/a:Alb}$ mouse livers were immunoblotted with the indicated antibodies. (B) The homogenates for which results are shown in panel A were fractionated by 10 to 40% glycerol gradient centrifugation and immunoblotted with the indicated antibodies. The faint Rpn10a bands detected in blots with anti-Rpn10(C) and anti-Rpn10(N) (asterisk) in the panels for Rpn10$^{a/a:Alb}$ liver are presumably derived from non-albumin-expressing cells in the liver. (C) The peptide-hydrolyzing activity of each fraction from panel B was measured as for Fig. 2F. (D) Real-time RT-PCR was used to measure the expression of transcripts encoding proteasome-related genes in the livers of 6-week-old Rpn10$^{a/a}$ and Rpn10$^{a/a:Alb}$ mice. Data represent levels of transcripts in Rpn10$^{a/a:Alb}$ liver relative to those in Rpn10$^{a/a}$ liver and are means ± standard deviations from experiments with three pairs of littermates. (E) The homogenates for which results are shown in panel A were immunoblotted with an anti-ubiquitin (Ub) antibody. (F) Ubiquitin-independent and -dependent protein-degrading activities of proteasomes. Homogenates from 6-week-old mouse livers were subjected to an in vitro protein degradation assay. Antizyme-dependent degradation of ^{35}S-labeled ODC (left) and ubiquitin-dependent degradation of ^{35}S-labeled cIAP1 (right) were measured. Data are means ± standard deviations from triplicate experiments. (G) Homogenates from Rpn10$^{a/a}$ and Rpn10$^{a/a:Alb}$ mouse livers were immunoprecipitated with an anti-Rpt6 antibody and subjected to immunoblotting with the indicated antibodies.

an increased amount of USP14 was detected in Rpn10ΔUIM proteasomes, consistent with the observation with yeast that ubiquitin stress enhances the loading of proteasomes with Ubp6, which is known to bind to 26S proteasomes via Rpn1 (14, 24). It is possible that USP14 competes with mHR23B for binding to proteasomes, specifically to Rpn1, although the binding of USP14 and mHR23B to mammalian Rpn1 has yet to be established. Therefore, we cannot evaluate the exact contribution of the UIM domain in accepting Rad23 in mammalian proteasomes. Whether ubiquitinated proteins are recognized directly by the UIM domains of Rpn10 or delivered to the UIM domain by Rad23 species, these results demonstrate that deletion of the UIM domains of Rpn10 causes insufficient delivery of ubiquitinated proteins to proteasomes, resulting in impairment of their degradation in mammals.

DISCUSSION

To date, genetic analysis of Rpn10 has been conducted on yeast, moss, plant, and fly (6, 9, 36, 38, 40, 41, 43). In the present study, we extended the genetic analysis of Rpn10 to vertebrates, employing gene-targeting techniques on mice. One of the aims of our study was to clarify the role of vertebrate-specific splice variants of Rpn10 (18). This was achieved by generating mice with Rpn10a knock-in and Rpn10b-to-Rpn10e knockout. Contrary to our expectation, Rpn10$^{a/a}$ mice did not show àny obvious defect throughout development, suggesting that the constitutive form of Rpn10 (i.e., Rpn10a) was sufficient at least for conventional development of mice. However, a previous report that analyzed Rpn10 variants in *Xenopus* suggested that specific interaction between Rpn10c and Scythe, a regulatory factor of Reaper-induced apoptosis, plays an important role in embryonic development (19). While our study was not designed to identify specific interacting molecules for mouse Rpn10 variants, it is possible that Rpn10 variants play some roles in more specific situations in mice.

Another aim of our study was to explore the role of Rpn10 in mice. Rpn10 deficiency is known to cause different phenotypes in different organisms. The severe developmental defects observed for Rpn10-deficient mice are in contrast to the viability of Rpn10-deficient yeast and worms but similar to the phenotypes observed for moss and flies, further confirming an essential role in higher eukaryotes. However, based on the phenotypes of ATPase subunit knockout mice, which exhibited an earlier halt in the developmental process than that for Rpn10 knockout mice (33), it is suggested that loss of Rpn10 could be compensated for to some degree, presumably by increasing transcription levels of proteasomes and UBL-UBA proteins as a feedback circuit in response to the accumulation of ubiquitinated proteins (40, 48).

The roles of the VWA and UIM domains of Rpn10 are also issues of debate. Rpn10ΔUIM mice, which express Rpn10 proteins lacking UIM domains but with the intact VWA domain, died in utero around E8.5, suggesting that the UIM-mediated recognition of ubiquitinated proteins is essential for mammalian development. Biochemical analysis of mice with liver-specific deletion of the UIM domains demonstrated accumulation of ubiquitinated proteins and defective proteolysis of ubiquitinated proteins. Considering that Rpn10ΔUIM mice survived longer than Rpn10-null mice, the VWA domain of Rpn10

might act as a "facilitator," as proposed for yeast (45). As shown in Fig. 4G, we detected a decreased amount of mHR23B in Rpn10ΔUIM proteasomes. Therefore, deletion of the UIM domains of Rpn10 impairs both direct binding and mHR23B-mediated delivery of ubiquitinated proteins to proteasomes. At present, the specific cause of the lethality of these mice in utero is not clear. Further studies are necessary to clarify whether such lethality is due to excessive general stress caused by accumulation of ubiquitinated proteins or to accumulation of some specific proteins that might essentially regulate mouse development, and in the latter case, what types of proteins these are.

ACKNOWLEDGMENTS

REFERENCES

1. Baumeister, W., J. Walz, F. Zuhl, and E. Seemuller. 1998. The proteasome: paradigm of a self-compartmentalizing protease. Cell 92:367–380.
2. Bertolaet, B. L., D. J. Clarke, M. Wolff, M. H. Watson, M. Henze, G. Divita, and S. I. Reed. 2001. UBA domains of DNA damage-inducible proteins interact with ubiquitin. Nat. Struct. Biol. 8:417–422.
3. Deveraux, Q., V. Ustrell, C. Pickart, and M. Rechsteiner. 1994. A 26S protease subunit that binds ubiquitin conjugates. J. Biol. Chem. 269:7059–7061.
4. Elsasser, S., D. Chandler-Militello, B. Muller, J. Hanna, and D. Finley. 2004. Rad23 and Rpn10 serve as alternative ubiquitin receptors for the proteasome. J. Biol. Chem. 279:26817–26822.
5. Elsasser, S., R. R. Gali, M. Schwickart, C. N. Larsen, D. S. Leggett, B. Muller, M. T. Feng, F. Tubing, G. A. Dittmar, and D. Finley. 2002. Proteasome subunit Rpn1 binds ubiquitin-like protein domains. Nat. Cell Biol. 4:725–730.
6. Fu, H., S. Sadis, D. M. Rubin, M. Glickman, S. van Nocker, D. Finley, and R. D. Vierstra. 1998. Multiubiquitin chain binding and protein degradation are mediated by distinct domains within the 26 S proteasome subunit Mcb1. J. Biol. Chem. 273:1970–1981.
7. Fujiwara, K., T. Tenno, K. Sugasawa, J. G. Jee, I. Ohki, C. Kojima, H. Tochio, H. Hiroaki, F. Hanaoka, and M. Shirakawa. 2004. Structure of the ubiquitin-interacting motif of S5a bound to the ubiquitin-like domain of HR23B. J. Biol. Chem. 279:4760–4767.
8. Funakoshi, M., T. Sasaki, T. Nishimoto, and H. Kobayashi. 2002. Budding yeast Dsk2p is a polyubiquitin-binding protein that can interact with the proteasome. Proc. Natl. Acad. Sci. USA 99:745–750.
9. Girod, P. A., H. Fu, J. P. Zryd, and R. D. Vierstra. 1999. Multiubiquitin chain binding subunit MCB1 (RPN10) of the 26S proteasome is essential for developmental progression in *Physcomitrella patens*. Plant Cell 11:1457–1472.
10. Glickman, M. H., and A. Ciechanover. 2002. The ubiquitin-proteasome proteolytic pathway: destruction for the sake of construction. Physiol. Rev. 82:373–428.
11. Glickman, M. H., D. M. Rubin, O. Coux, I. Wefes, G. Pfeifer, Z. Cjeka, W. Baumeister, V. A. Fried, and D. Finley. 1998. A subcomplex of the proteasome regulatory particle required for ubiquitin-conjugate degradation and related to the COP9-signalosome and eIF3. Cell 94:615–623.
12. Glockzin, S., F. X. Ogi, A. Hengstermann, M. Scheffner, and C. Blattner. 2003. Involvement of the DNA repair protein hHR23 in p53 degradation. Mol. Cell. Biol. 23:8960–8969.
13. Hamazaki, J., S. Iemura, T. Natsume, H. Yashiroda, K. Tanaka, and S. Murata. 2006. A novel proteasome interacting protein recruits the deubiquitinating enzyme UCH37 to 26S proteasomes. EMBO J. 25:4524–4536.
14. Hanna, J., A. Meides, D. P. Zhang, and D. Finley. 2007. A ubiquitin stress response induces altered proteasome composition. Cell 129:747–759.
15. Hershko, A., and A. Ciechanover. 1998. The ubiquitin system. Annu. Rev. Biochem. 67:425–479.
16. Hirano, Y., K. B. Hendil, H. Yashiroda, S. Iemura, R. Nagane, Y. Hioki, T. Natsume, K. Tanaka, and S. Murata. 2005. A heterodimeric complex that promotes the assembly of mammalian 20S proteasomes. Nature 437:1381–1385.
17. Hiyama, H., M. Yokoi, C. Masutani, K. Sugasawa, T. Maekawa, K. Tanaka, J. H. Hoeijmakers, and F. Hanaoka. 1999. Interaction of hHR23 with S5a. The ubiquitin-like domain of hHR23 mediates interaction with S5a subunit of 26 S proteasome. J. Biol. Chem. 274:28019–28025.

18. Kawahara, H., M. Kasahara, A. Nishiyama, K. Ohsumi, T. Goto, T. Kishimoto, Y. Saeki, H. Yokosawa, N. Shimbara, S. Murata, T. Chiba, K. Suzuki, and K. Tanaka. 2000. Developmentally regulated, alternative splicing of the Rpn10 gene generates multiple forms of 26S proteasomes. EMBO J. 19:4144–4153.

19. Kikukawa, Y., R. Minami, M. Shimada, M. Kobayashi, K. Tanaka, H. Yokosawa, and H. Kawahara. 2005. Unique proteasome subunit Xrpn10c is a specific receptor for the antiapoptotic ubiquitin-like protein Scythe. FEBS J. 272:6373–6386.

20. Kim, I., K. Mi, and H. Rao. 2004. Multiple interactions of rad23 suggest a mechanism for ubiquitylated substrate delivery important in proteolysis. Mol. Biol. Cell 15:3357–3365.

21. Kleijnen, M. F., R. M. Alarcon, and P. M. Howley. 2003. The ubiquitin-associated domain of hPLIC-2 interacts with the proteasome. Mol. Biol. Cell 14:3868–3875.

22. Lakso, M., J. G. Pichel, J. R. Gorman, B. Sauer, Y. Okamoto, E. Lee, F. W. Alt, and H. Westphal. 1996. Efficient in vivo manipulation of mouse genomic sequences at the zygote stage. Proc. Natl. Acad. Sci. USA 93:5860–5865.

23. Lambertson, D., L. Chen, and K. Madura. 1999. Pleiotropic defects caused by loss of the proteasome-interacting factors Rad23 and Rpn10 of Saccharomyces cerevisiae. Genetics 153:69–79.

24. Leggett, D. S., J. Hanna, A. Borodovsky, B. Crosas, M. Schmidt, R. T. Baker, T. Walz, H. Ploegh, and D. Finley. 2002. Multiple associated proteins regulate proteasome structure and function. Mol. Cell 10:495–507.

25. Mueller, T. D., and J. Feigon. 2003. Structural determinants for the binding of ubiquitin-like domains to the proteasome. EMBO J. 22:4634–4645.

26. Murakami, Y., S. Matsufuji, T. Kameji, S. Hayashi, K. Igarashi, T. Tamura, K. Tanaka, and A. Ichihara. 1992. Ornithine decarboxylase is degraded by the 26S proteasome without ubiquitination. Nature 360:597–599.

27. Murata, S., H. Kawahara, S. Tohma, K. Yamamoto, M. Kasahara, Y. Nabeshima, K. Tanaka, and T. Chiba. 1999. Growth retardation in mice lacking the proteasome activator PA28γ. J. Biol. Chem. 274:38211–38215.

28. Postic, C., M. Shiota, K. D. Niswender, T. L. Jetton, Y. Chen, J. M. Moates, K. D. Shelton, J. Lindner, A. D. Cherrington, and M. A. Magnuson. 1999. Dual roles for glucokinase in glucose homeostasis as determined by liver and pancreatic beta cell-specific gene knock-outs using Cre recombinase. J. Biol. Chem. 274:305–315.

29. Qiu, X. B., S. Y. Ouyang, C. J. Li, S. Miao, L. Wang, and A. L. Goldberg. 2006. hRpn13/ADRM1/GP110 is a novel proteasome subunit that binds the deubiquitinating enzyme, UCH37. EMBO J. 25:5742–5753.

30. Richly, H., M. Rape, S. Braun, S. Rumpf, C. Hoege, and S. Jentsch. 2005. A series of ubiquitin binding factors connects CDC48/p97 to substrate multiubiquitylation and proteasomal targeting. Cell 120:73–84.

31. Saeki, Y., A. Saitoh, A. Toh-e, and H. Yokosawa. 2002. Ubiquitin-like proteins and Rpn10 play cooperative roles in ubiquitin-dependent proteolysis. Biochem. Biophys. Res. Commun. 293:986–992.

32. Saeki, Y., T. Sone, A. Toh-e, and H. Yokosawa. 2002. Identification of ubiquitin-like protein-binding subunits of the 26S proteasome. Biochem. Biophys. Res. Commun. 296:813–819.

33. Sakao, Y., T. Kawai, O. Takeuchi, N. G. Copeland, D. J. Gilbert, N. A. Jenkins, K. Takeda, and S. Akira. 2000. Mouse proteasomal ATPases Psmc3 and Psmc4: genomic organization and gene targeting. Genomics 67:1–7.

34. Schauber, C., L. Chen, P. Tongaonkar, I. Vega, D. Lambertson, W. Potts, and K. Madura. 1998. Rad23 links DNA repair to the ubiquitin/proteasome pathway. Nature 391:715–718.

35. Seeger, M., R. Hartmann-Petersen, C. R. Wilkinson, M. Wallace, I. Samejima,

M. S. Taylor, and C. Gordon. 2003. Interaction of the anaphase-promoting complex/cyclosome and proteasome protein complexes with multiubiquitin chain-binding proteins. J. Biol. Chem. 278:16791–16796.

36. Shimada, M., K. Kanematsu, K. Tanaka, H. Yokosawa, and H. Kawahara. 2006. Proteasomal ubiquitin receptor RPN-10 controls sex determination in Caenorhabditis elegans. Mol. Biol. Cell 17:5356–5371.

37. Silke, J., T. Kratina, D. Chu, P. G. Ekert, C. L. Day, M. Pakusch, D. C. Huang, and D. L. Vaux. 2005. Determination of cell survival by RING-mediated regulation of inhibitor of apoptosis (IAP) protein abundance. Proc. Natl. Acad. Sci. USA 102:16182–16187.

38. Smalle, J., J. Kurepa, P. Yang, T. J. Emborg, E. Babiychuk, S. Kushnir, and R. D. Vierstra. 2003. The pleiotropic role of the 26S proteasome subunit RPN10 in Arabidopsis growth and development supports a substrate-specific function in abscisic acid signaling. Plant Cell 15:965–980.

39. Smith, D. M., G. Kafri, Y. Cheng, D. Ng, T. Walz, and A. L. Goldberg. 2005. ATP binding to PAN or the 26S ATPases causes association with the 20S proteasome, gate opening, and translocation of unfolded proteins. Mol. Cell 20:687–698.

40. Szlanka, T., L. Haracska, I. Kiss, P. Deak, E. Kurucz, I. Ando, E. Viragh, and A. Udvardy. 2003. Deletion of proteasomal subunit S5a/Rpn10/p54 causes lethality, multiple mitotic defects and overexpression of proteasomal genes in Drosophila melanogaster. J. Cell Sci. 116:1023–1033.

41. Takahashi, M., H. Iwasaki, H. Inoue, and K. Takahashi. 2002. Reverse genetic analysis of the Caenorhabditis elegans 26S proteasome subunits by RNA interference. Biol. Chem. 383:1263–1266.

42. Tanaka, K., and M. Kasahara. 1998. The MHC class I ligand-generating system: roles of immunoproteasomes and the interferon-γ-inducible proteasome activator PA28. Immunol. Rev. 163:161–176.

43. van Nocker, S., S. Sadis, D. M. Rubin, M. Glickman, H. Fu, O. Coux, I. Wefes, D. Finley, and R. D. Vierstra. 1996. The multiubiquitin-chain-binding protein Mcb1 is a component of the 26S proteasome in Saccharomyces cerevisiae and plays a nonessential, substrate-specific role in protein turnover. Mol. Cell. Biol. 16:6020–6028.

44. Verma, R., L. Aravind, R. Oania, W. H. McDonald, J. R. Yates III, E. V. Koonin, and R. J. Deshaies. 2002. Role of Rpn11 metalloprotease in deubiquitination and degradation by the 26S proteasome. Science 298:611–615.

45. Verma, R., R. Oania, J. Graumann, and R. J. Deshaies. 2004. Multiubiquitin chain receptors define a layer of substrate selectivity in the ubiquitin-proteasome system. Cell 118:99–110.

46. Walters, K. J., P. J. Lech, A. M. Goh, Q. Wang, and P. M. Howley. 2003. DNA-repair protein hHR23a alters its protein structure upon binding proteasomal subunit S5a. Proc. Natl. Acad. Sci. USA 100:12694–12699.

47. Watt, A. J., M. A. Battle, J. Li, and S. A. Duncan. 2004. GATA4 is essential for formation of the proepicardium and regulates cardiogenesis. Proc. Natl. Acad. Sci. 101:12573–12578.

48. Xie, Y., and A. Varshavsky. 2001. RPN4 is a ligand, substrate, and transcriptional regulator of the 26S proteasome: a negative feedback circuit. Proc. Natl. Acad. Sci. USA 98:3056–3061.

49. Yao, T., and R. E. Cohen. 2002. A cryptic protease couples deubiquitination and degradation by the proteasome. Nature 419:403–407.

50. Yao, T., L. Song, W. Xu, G. N. DeMartino, L. Florens, S. K. Swanson, M. P. Washburn, R. C. Conaway, J. W. Conaway, and R. E. Cohen. 2006. Proteasome recruitment and activation of the Uch37 deubiquitinating enzyme by Adrm1. Nat. Cell Biol. 8:994–1002.

Homeostatic Levels of p62 Control Cytoplasmic Inclusion Body Formation in Autophagy-Deficient Mice

Masaaki Komatsu,[1,2,3] Satoshi Waguri,[4] Masato Koike,[5] Yu-shin Sou,[1,2] Takashi Ueno,[2] Taichi Hara,[6] Noboru Mizushima,[6,7] Jun-ichi Iwata,[1,2] Junji Ezaki,[2] Shigeo Murata,[1] Jun Hamazaki,[1] Yasumasa Nishito,[1] Shun-ichiro Iemura,[8] Tohru Natsume,[8] Toru Yanagawa,[9] Junya Uwayama,[9] Eiji Warabi,[9] Hiroshi Yoshida,[9] Tetsuro Ishii,[9] Akira Kobayashi,[10] Masayuki Yamamoto,[10] Zhenyu Yue,[11] Yasuo Uchiyama,[5] Eiki Kominami,[2] and Keiji Tanaka[1,*]

[1]Laboratory of Frontier Science, Tokyo Metropolitan Institute of Medical Science, Bunkyo-ku, Tokyo 113-8613, Japan
[2]Department of Biochemistry, Juntendo University School of Medicine, Bunkyo-ku, Tokyo 113-8421, Japan
[3]PRESTO, Japan Science and Technology Corporation, Kawaguchi 332-0012, Japan
[4]Department of Anatomy and Histology, Fukushima Medical University School of Medicine, Hikarigaoka, Fukushima 960-1295, Japan
[5]Department of Cell Biology and Neurosciences, Osaka University Graduate School of Medicine, Suita, Osaka 565-0871, Japan
[6]Department of Physiology and Cell Biology, Tokyo Medical and Dental University Graduate School and Faculty of Medicine, Bunkyo-ku, Tokyo 113-8519, Japan
[7]SORST, Japan Science and Technology Corporation, Kawaguchi 332-0012, Japan
[8]National Institutes of Advanced Industrial Science and Technology, Biological Information Research Center (JBIRC), Kohtoh-ku, Tokyo 135-0064, Japan
[9]Graduate School of Comprehensive Human Sciences, University of Tsukuba, Tennoudai, Tsukuba 305-8575, Japan
[10]Department of Medical Biochemistry and ERATO-JST, Tohoku University Graduate School of Medicine, Aoba-ku, Sendai 980-8575, Japan
[11]Departments of Neurology and Neuroscience, Mount Sinai School of Medicine, New York, NY 10029, USA
*Correspondence: tanakak@rinshoken.or.jp
DOI 10.1016/j.cell.2007.10.035

SUMMARY

Inactivation of constitutive autophagy results in formation of cytoplasmic protein inclusions and leads to liver injury and neurodegeneration, but the details of abnormalities related to impaired autophagy are largely unknown. Here we used mouse genetic analyses to define the roles of autophagy in the aforementioned events. We report that the ubiquitin- and LC3-binding protein "p62" regulates the formation of protein aggregates and is removed by autophagy. Thus, genetic ablation of p62 suppressed the appearance of ubiquitin-positive protein aggregates in hepatocytes and neurons, indicating that p62 plays an important role in inclusion body formation. Moreover, loss of p62 markedly attenuated liver injury caused by autophagy deficiency, whereas it had little effect on neuronal degeneration. Our findings highlight the unexpected role of homeostatic level of p62, which is regulated by autophagy, in controlling intracellular inclusion body formation, and indicate that the pathologic process associated with autophagic deficiency is cell-type specific.

INTRODUCTION

Macroautophagy (hereafter referred to as autophagy) is a highly conserved bulk protein degradation pathway in eukaryotes. In the initial step of this process, the cytoplasmic portions and organelles are engulfed within a double-membrane vesicle called autophagosome, and then the autophagosome fuses with the lysosomes to degrade the sequestered materials by various lysosomal hydrolytic enzymes, followed by generation of amino acids that are recycled for macromolecular synthesis and energy production. Emerging evidence emphasizes the importance of autophagy in various biological and pathological processes, such as cellular remodeling, tumorigenesis, and developmental programs (Levine and Klionsky, 2004).

Recent evidence indicates that in mammalian cells, autophagy serves two physiological purposes. The first is to supply amino acids for cell survival under poor environmental conditions, which is universally known as "adaptive autophagy." Indeed, this type of autophagy is rapidly induced under nutritional deprivation in yeast (Tsukada and Ohsumi, 1993) and in newborn mice (Kuma et al., 2004), serving as a basic survival strategy in all eukaryotes. The second is to degrade proteins in the cell through continuous operation at a low level irrespective of nutritional stress, known as "basal or constitutive autophagy." In the latter pathway, autophagy is responsible for the

turnover of long-lived proteins, disposal of excess (Iwata et al., 2006) or damaged organelles (Elmore et al., 2001), and clearance of aggregate-prone proteins (Fortun et al., 2003; Kamimoto et al., 2006; Ravikumar et al., 2004). Recent genetic studies using mice have highlighted the importance of constitutive autophagy in nondividing cells, such as hepatocytes and neurons, in which loss of autophagy results in severe liver injury and neurodegeneration, respectively (Hara et al., 2006; Komatsu et al., 2005, 2006). Unexpected findings in these studies were that loss of autophagy causes cytoplasmic accumulation of ubiquitin-positive proteinaceous inclusions, together with hepatocytic and neuronal death without expression of proteins with disease-associated mutations (Hara et al., 2006; Komatsu et al., 2005, 2006). However, the underlying mechanism of inclusion body formation in the aforementioned diseases is largely unknown at present.

Using mouse genetics, we report the critical role of the multifunctional protein "p62/A170/SQSTM1" (also known as a signaling adaptor/scaffold protein) in the formation of intracellular ubiquitin-related protein aggregation caused by deficiency in autophagy. We show that autophagic degradation of the "p62" via direct interaction with LC3, a posttranslational modifier essential for autophagosome formation, prevents inclusion body formation. Importantly, our studies uncover the molecular mechanism linking autophagy, p62, and inclusion body formation, which is a cellular hallmark in various pathophysiological conditions, and reveal pathophysiological changes associated with loss of p62 and/or autophagy in hepatocytes and neurons.

RESULTS

Identification of LC3-Interacting Proteins

The microtubule-associated protein 1A/1B *light chain 3* (LC3) is a modifier protein conjugated with phosphatidyl-ethanolamine (PE), analogous to Atg8 in yeast (Ichimura et al., 2000). PE-conjugated LC3 (LC3-II) is localized in the inner and outer membranes of autophagosomes, and the population associated with the inner membrane is degraded after fusion of autophagosomes with lysosomes (Kabeya et al., 2000). To identify protein(s) that could interact with LC3, we employed the proteomic approach as described previously (Komatsu et al., 2004) and then identified a unique protein p62 as one of LC3-interacting proteins, in addition to LC3-modifying enzymes (Ohsumi, 2001) (Table S1). The p62 protein is conserved in metazoa and plants but not in yeasts and can bind a large number of proteins through its multiple protein-protein interaction motifs (Moscat et al., 2006) (Figure S1). This protein mediates diverse signaling pathways including cell stress, survival, and inflammation (Moscat et al., 2006; Wooten et al., 2006).

p62 Is Degraded by Autophagy-Lysosome Pathway

To verify the interaction between LC3 and p62 in vivo, we first carried out immunoprecipitation assay with cultured hepatocytes isolated from green fluorescent protein (GFP)-LC3 transgenic (Tg) mice (GFP-LC3 tg) (Mizushima et al., 2004) and confirmed the coimmunoprecipitation of p62 with GFP-LC3 under both nutrient-rich and -poor conditions (Figure 1A). We also confirmed the coimmunoprecipitation of p62 with endogenous LC3 in wild-type mouse liver (Figure 1B). In addition to the major band, the minor band detected by our p62 antibody was probably a p62 splicing variant product found in the mouse protein database or a partially cleaved product (see also Figures 2, 3, and 4). Moreover, recombinant p62 was pulled down with recombinant GST-LC3 (Figure 1C), indicating direct physical interaction between p62 and LC3. Subsequent binding assays with a series of recombinant p62 mutants indicated that p62 interacts with LC3 through a linker region that connects the N-terminal Zinc finger and the C-terminal *ub*iquitin-associated (UBA) domain of p62 (Figure S1). Immunofluorescence microscopy using hepatocytes isolated from GFP-LC3 Tg mice showed colocalization of large numbers of punctate signal for GFP-LC3 (84.7% ± 10.9%, ± SD, n = 21) with that for p62 (Figure 1E). When autophagosome formation was induced by nutrient-deprivation, 34.9% ± 6.7% (n = 22) of ring-shaped GFP-LC3-positive autophagosomes contained p62 signal, some of which showed partial colocalization (Figure 1F). A similar colocalization pattern was also observed in liver sections of GFP-LC3 Tg starved for 1 day (Figure 1G). The p62-positive and GFP-LC3-negative particles might correspond to late endosomes or lysosomes, as reported previously (Sanchez et al., 1998). Consistent with the notion that some population of LC3-II is degraded in lysosomes (Kabeya et al., 2000), treatment with lysosomal enzyme inhibitors, but not with a proteasomal inhibitor, resulted in the accumulation of LC3-II in primary hepatocytes (Figure 1D). Similarly, lysosomal inhibition resulted in marked accumulation of p62 (Figure 1D). When lysosomal inhibitors were added to cultured hepatocytes, the majority of p62 accumulated around the perinuclear region, where it colocalized with the lysosomal marker LysoTracker (Figure 1H), suggesting the turnover of p62 together with LC3II in lysosomes.

p62 Is a Component of Inclusions in Autophagy-Deficient Hepatocytes

If p62 is degraded by the autophagic-lysosome pathway, autophagy deficiency should result in the accumulation of p62 protein. To test this in vivo, we used the $Atg7^{F/F}$:Mx1 mice, in which $Atg7$, a gene essential for autophagy, can be depleted in the liver by intraperitoneal injections of polyinosinic acid-polycytidylic acid (pIpC) (Figure 2A, left panel) (Komatsu et al., 2005). We observed specific accumulation of p62 protein in $Atg7$-deficient livers (Figures 2A and 2D) without marked induction of p62 mRNA (Figure 2E). Similar to $Atg7$ knockout liver, deficiency of $Atg5$, which is essential for autophagosome formation (Mizushima et al., 2001), was also associated with marked accumulation of p62 (Figure S2). These results indicate that p62 turnover is mediated by autophagy. Autophagic
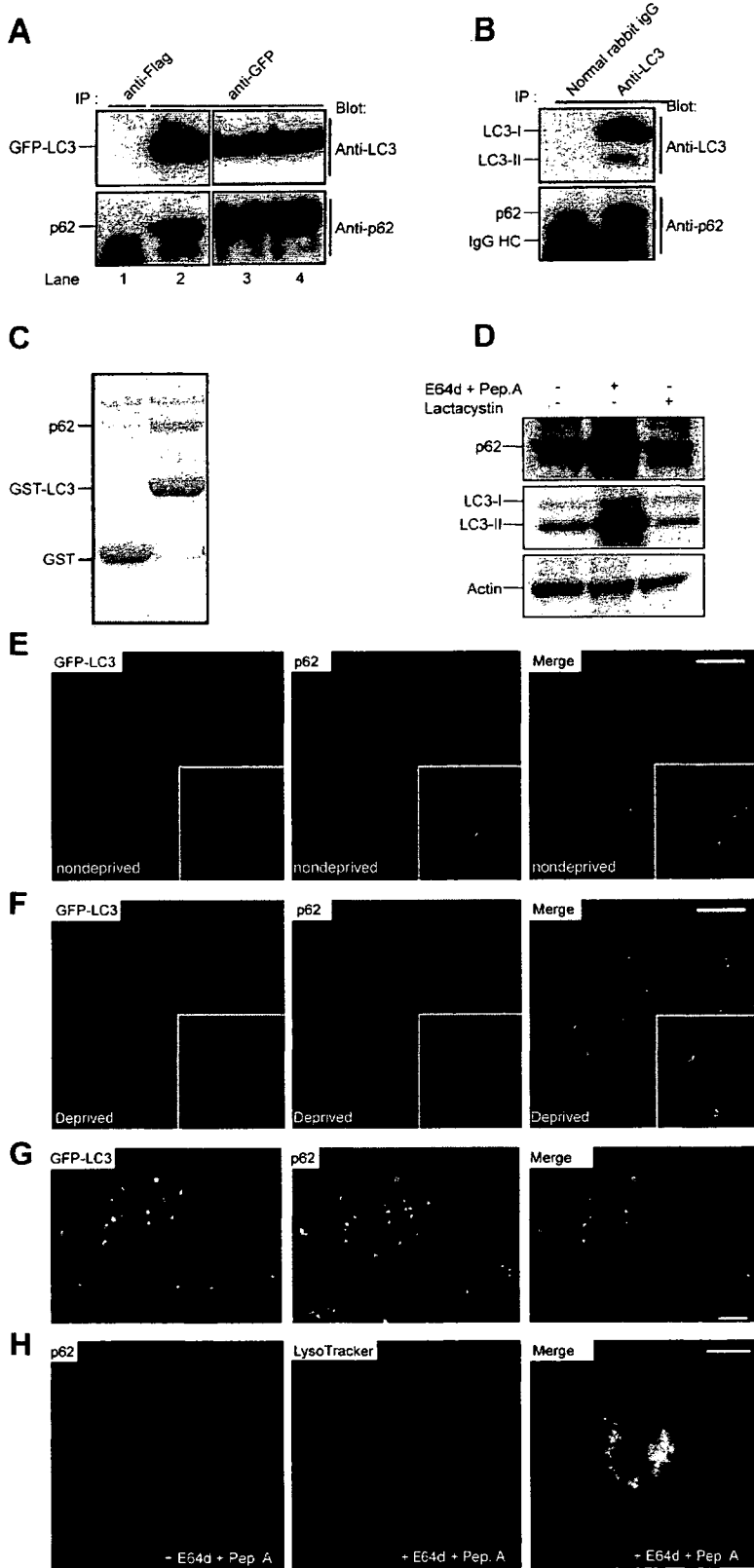
A

IP: anti-Flag   anti-GFP

GFP-LC3—

p62—

Lane   1   2   3   4

Blot:

Anti-LC3

Anti-p62

B

IP: Normal rabbit IgG   Anti-LC3

LC3-I—
LC3-II—

p62—
IgG HC—

Blot:

Anti-LC3

Anti-p62

C

p62—

GST-LC3—

GST—

D

E64d + Pep.A   -   +   -
Lactacystin   -   -   +

p62—

LC3-I—
LC3-II—

Actin—

E

GFP-LC3   p62   Merge

nondeprived   nondeprived   nondeprived

F

GFP-LC3   p62   Merge

Deprived   Deprived   Deprived

G

GFP-LC3   p62   Merge

H

p62   LysoTracker   Merge

- E64d + Pep A   + E64d + Pep. A   - E64d + Pep A

Figure 1. p62 Is Degraded by the Autophagic-Lysosomal Pathway

(A) Interaction of p62 with GFP-LC3. Hepatocytes prepared from GFP-LC3 Tg mice were cultured for 3 hr in Williams' E medium (lanes 1, 2, and 3) or Hank's solution (lane 4). The cell lysates were immunoprecipitated with anti-Flag or GFP antibodies followed by immunoblotting with antibodies against LC3 and p62.

(B) Interaction of p62 with endogenous LC3. Liver lysates from wild-type mice were immunoprecipitated with anti-LC3 antibody or normal rabbit IgG followed by immunoblotting with antibodies against LC3 and p62.

(C) In vitro GST pull-down analysis of purified p62 by recombinant GST or GST-LC3.

(D) Degradation of p62 and LC3. Hepatocytes prepared from wild-type mice were treated with E64d (10 μg/ml) and pepstatin A (10 μg/ml) for 24 hr or lactacystin (10 μM) for 3 hr. The cell lysates were subjected to SDS-PAGE followed by immunoblotting with indicated antibodies. Data shown in (A)–(D) are representative of three separate experiments.

(E, F, and H) Immunofluorescent analysis of primary cultured hepatocytes. Hepatocytes isolated from GFP-LC3 Tg mice were cultured for 3 hr in Williams' E medium (E) and Hank's solution (F) or for 24 hr in Williams' E with E64d and pepstatin A (H) and then immunostained with antibody against p62. Lysosomal inhibitor-treated hepatocytes were stained with the fluorescent acidotropic probe LysoTracker prior to p62 immunostaining (H). Higher magnification views are shown in insets. Bar, 10 μm.

(G) Immunofluorescence analysis of the liver of GFP-LC3 Tg mice. Mice were fasted for 1 day, and then the liver sections were immunostained with anti-p62 antibody. Right panels show merged images. Bar, 10 μm.
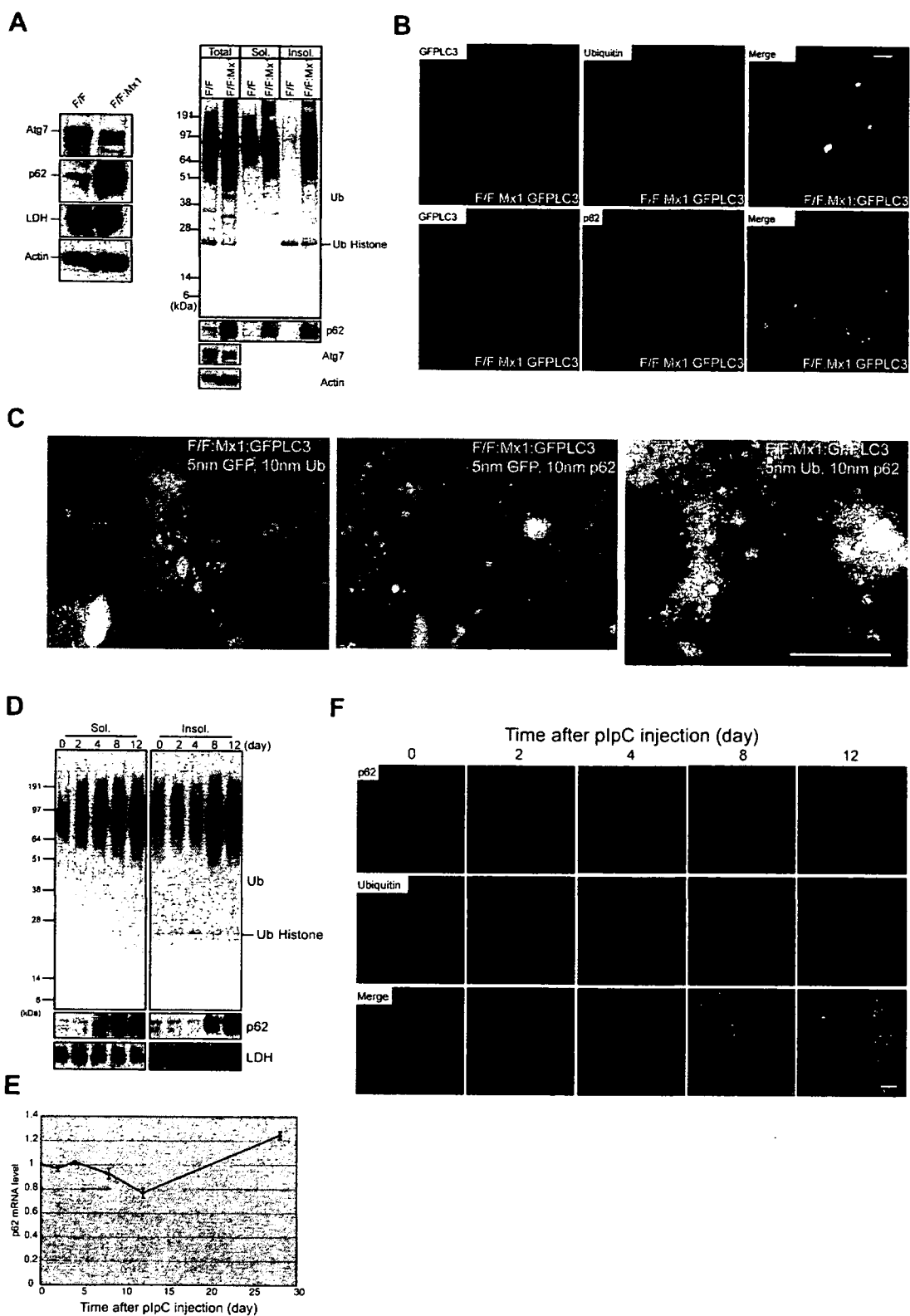
A

B

C

D

E

F

Figure 2. Formation of Ubiquitin- and p62-Positive Inclusions in Autophagy-Deficient Hepatocytes

(A) Accumulation of p62 in Atg7-deficient hepatocytes. Left panel shows liver homogenates from Atg7$^{F/F}$ and Atg7$^{F/F}$:Mx1 mice at 28-day post-pIpC injection were subjected to SDS-PAGE followed by immunoblotting with indicated antibodies. Right panel shows liver homogenates were separated

breakdown of p62 appears to occur irrespective of cell type, because a similar observation was recently reported in HeLa, HEK293T, and mouse embryonic fibroblasts (Bjorkoy et al., 2005; Wang et al., 2006).

Interestingly, abundant amounts of p62 were noted in both detergent-soluble and insoluble fractions from Atg7-deficient livers (Figure 2A, right-middle panel), in parallel with accumulation of ubiquitinated proteins in both fractions from Atg7-deficient but not from control livers (Figure 2A, right-top panel) (Komatsu et al., 2005). Subsequently, to investigate the cellular localization of ubiquitin, p62, and LC3 in autophagy-deficient hepatocytes, we generated the $Atg7^{F/F}$:Mx1:GFP-LC3 mice by crossing $Atg7^{F/F}$:Mx1 with GFP-LC3 Tg mice. Immunofluorescence microscopy showed that the Atg7-deficient cultured hepatocytes contained abundant ubiquitin- (Figure 2B, top panels), or p62- (Figure 2B, bottom panels) positive inclusions in the cytoplasm, which were also positive for GFP-LC3. Finally, double immunoelectron microscopy confirmed the colocalization of LC3, ubiquitin, and p62 proteins in the cytoplasmic aggregated structures (Figures 2C and S3). Next, we analyzed the inclusion formation process. Immunoblot analysis revealed that p62 began to accumulate in the detergent-soluble fraction at 4 days and was abundant in both detergent-soluble and -insoluble fractions at 8 days (Figure 2D). In contrast, RT-PCR analysis showed no induction of p62 transcript during this period (Figure 2E). The accumulation pattern of polyubiquitinated proteins essentially matched that of p62 (Figure 2D). Double-immunofluorescence microscopy showed the appearance of ubiquitin- and p62-double-positive dots at 2 days in some $Atg7^{F/F}$:Mx1 hepatocytes (Figure 2F). At later stages, both the number of hepatocytes containing the inclusions and the size of the inclusions increased gradually with time. These results suggest the time-dependent development of inclusions containing both ubiquitin and p62 in autophagy-deficient hepatocytes.

p62 Is a Component of Inclusions in Autophagy-Deficient Neurons

Next, we investigated the behavior of p62 in neuronal-specific autophagy-deficient mice, $Atg7^{F/F}$:Nes mice

(Komatsu et al., 2006). Similar to autophagy-deficient livers, p62 accumulated in the mutant brain without the apparent induction of its mRNA (Figures 3A and 3B), implying a common pathway in p62 turnover across tissues. Furthermore, the p62-positive inclusions were observed immunohistochemically in various brain regions in $Atg7^{F/F}$:Nes mice (Figure S4). Double-immunofluorescence microscopy revealed extensive colocalization of p62 and LC3 (Figure 3C, left panels), or p62 and ubiquitin (Figure 3C, right panels), in numerous inclusions in the cerebral cortex. Immunoelectron microscopy confirmed the localization of p62 in the cytoplasmic aggregated structures (Figures 3D, top panel, and S5). These inclusions also contained ubiquitin (Figures 3D, bottom panel, and S5). Next, we investigated the time course of inclusion formation in the cerebral cortex of $Atg7^{F/F}$:Nes mice from 2 to 28 days after birth. Ubiquitin/p62-double-positive dots began to appear at postnatal day 2 in the cerebral cortex, and they increased in size and number during postnatal development (Figure 3E). Taken together, these results indicate that reduced autophagic activity leads to the formation of ubiquitin- and p62-double positive inclusions in neurons.

Generation of p62-Knockout Mice

To examine the physiological roles of p62 in autophagy, we generated p62-knockout ($p62^{-/-}$) mice (Figure S6). They were born at Mendelian frequency, fertile and lived longer than 1 year (data not shown). Although p62 deficiency was associated with adulthood-onset obesity and diabetes as reported recently (Rodriguez et al., 2006), no apparent abnormality was noted in the p62-deleted liver (Figure S7). Moreover, p62-deficient mice exhibited neither marked neurodegeneration nor inclusion formation in neurons (see Figures 6 and S8). The conversion from LC3-I to LC3-II, induction of GFP-LC3 dots, and the appearance of many autophagosome structures after starvation were similar between the control and p62-deficient hepatocytes (Figures S9A, S9B, and S9C). Furthermore, there was no significant change in the turnover of long-lived protein in the mutant hepatocytes (Figure S9D).

---

into detergent (0.5% Tx-100)-soluble (Sol.) and insoluble (Insol.) fractions. Each fraction was subjected to SDS-PAGE and analyzed by immunoblotting with indicated antibodies. Data shown are representative of three separate experiments.

(B) Immunofluorescence analysis of cellular localization of ubiquitin, p62, and LC3 in autophagy-deficient hepatocytes. Hepatocytes isolated from $Atg7^{F/F}$:Mx1:GFP-LC3 mice at 14-day post-pIpC injection were immunostained with anti-ubiquitin or p62 antibodies. Right panels show merged images. Bar, 10 μm.

(C) Immunoelectron micrograph showing double labeling of ubiquitin (10 nm colloidal gold particles [cgp]) and GFP (5 nm cgp), p62 (10 nm cgp), and GFP (5 nm cgp), or p62 (10 nm cgp) and ubiquitin (5 nm cgp) in hepatocytes isolated from $Atg7^{F/F}$:Mx1:GFP-LC3 mice at 14-day post-pIpC injection. Bars, 0.5 μm. Magnified images can be seen in Figure S3.

(D) Immunoblotting analyses of ubiquitinated proteins and p62 in $Atg7^{F/F}$:Mx1 mice livers at various time points post-pIpC injection. Each fraction prepared as shown in (A) was subjected to SDS-PAGE and analyzed by immunoblotting with indicated antibodies. Data shown are representative of three separate experiments.

(E) Quantitation of p62 mRNA level in $Atg7^{F/F}$:Mx1 liver by RT-PCR. Total RNAs were prepared from $Atg7^{F/F}$:Mx1 livers at various time points post-pIpC injection, and then cDNA was synthesized from each RNA, followed by real-time PCR analysis. Data are mean ± standard deviation (SD) values of p62 mRNA normalized to the amount in $Atg7^{F/F}$:Mx1 liver at 0 day post-pIpC injection.

(F) Immunohistochemical detection of p62- and ubiquitin-positive inclusions in Atg7-deficient livers. $Atg7^{F/F}$:Mx1 mice were sacrificed at various time points post-pIpC injection, and liver sections were immunostained with anti-ubiquitin and p62 antibodies. Bottom panels show merged images. Bar, 10 μm.
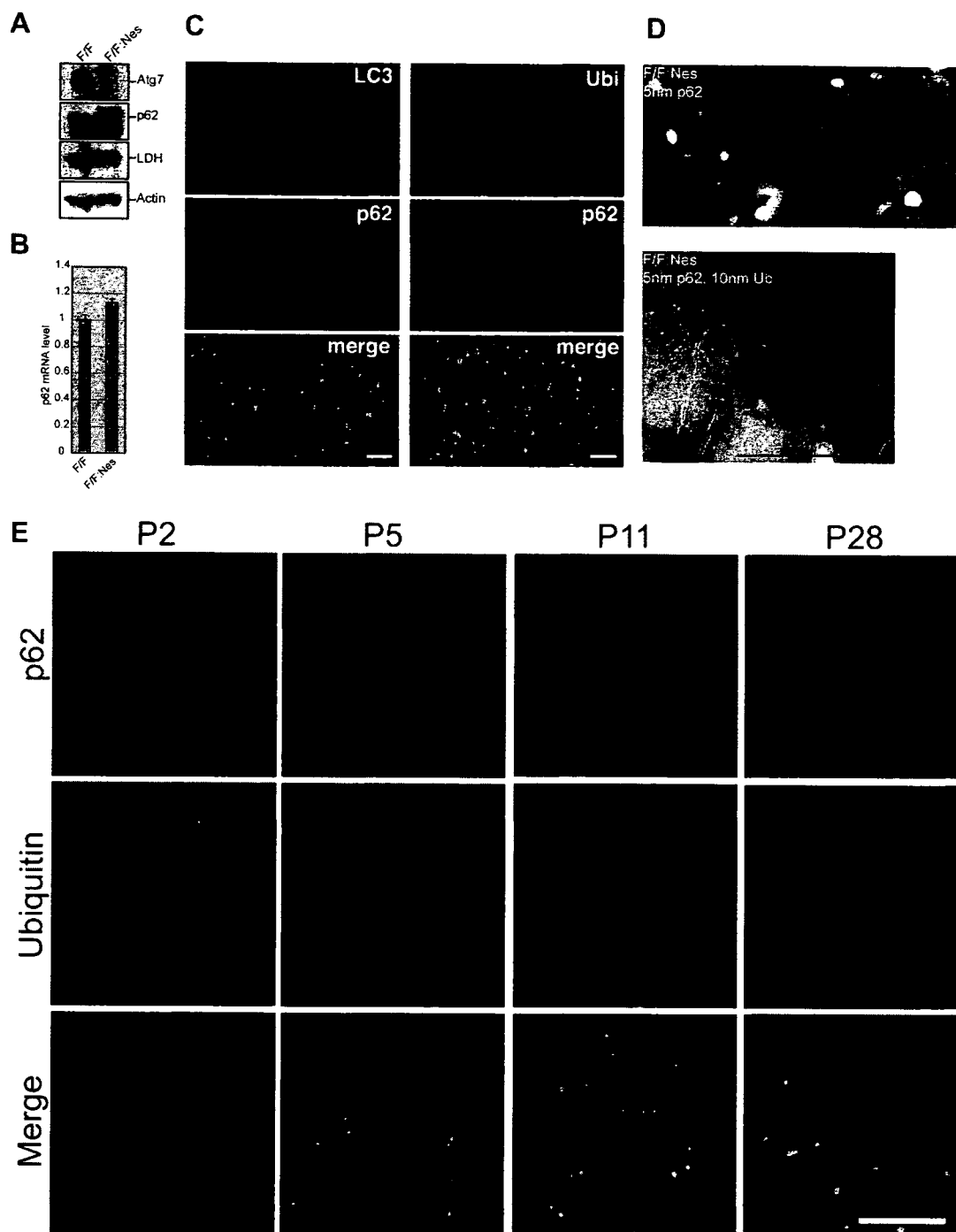
Figure 3. Formation of Ubiquitin- and p62-Positive Inclusions in Autophagy-Deficient Neurons

(A) Accumulation of p62 in Atg7-deficient brains. Brain homogenates from $Atg7^{F/F}$ and $Atg7^{F/F}$:Nes mice at 8 weeks of age were subjected to SDS-PAGE and analyzed by immunoblotting with indicated antibodies. Data shown are representative of three separate experiments.

(B) Quantitation of p62 mRNA level in Atg7-deficient brains by RT-PCR. Total RNAs were prepared from brains of $Atg7^{F/F}$ and $Atg7^{F/F}$:Nes mice at 8 weeks of age and analyzed as shown in Figure 2E. Data are mean ± SD values of p62 mRNA normalized to the amount in $Atg7^{F/F}$ brain. The experiments were performed three times.

(C) Immunofluorescence microscopy in $Atg7^{F/F}$:Nes cerebral cortex. Brain sections of $Atg7^{F/F}$:Nes mice were immunostained with anti-LC3 and p62 antibodies (left panels) or anti-ubiquitin and p62 antibodies (right panels). Bottom panels show merged images. Bar, 10 μm.

(D) Immunoelectron micrograph showing labeling of p62 (top panel) or double labeling of ubiquitin (10 nm cgp) and p62 (5 nm cgp) in hypothalamic neurons of 8-week-old $Atg7^{F/F}$:Nes mice. Bars, 0.5 μm. Magnified images can be seen in Figure S5.

Loss of p62 Suppresses Inclusion Formation in Autophagy-Deficient Hepatocytes

Next, to investigate the roles of p62 in inclusion formation, we crossed $Atg7^{F/F}$:Mx1 with $p62^{-/-}$ mice, producing the $Atg7$- and $p62$-double knockout (DKO) mice ($Atg7^{F/F}$: Mx1:$p62^{-/-}$). In contrast to large number of inclusions positive for ubiquitin in $Atg7$-deficient hepatocytes, surprisingly such ubiquitin inclusions were almost completely dispersed in the DKO hepatocytes (Figure 4A). Immunoblot analysis revealed that the amounts of accumulated polyubiquitinated proteins in DKO liver were lower than those in $Atg7$-deficient liver. Moreover, the reduction was more prominent in the insoluble fraction (Figures 4B and S10A). Interestingly, proteasome function evaluated by the degradation of polyubiquitinated protein was not significantly different among the genotypes (Figure S11A). Furthermore, the degradation of long-lived protein in DKO hepatocytes was significantly reduced to the levels as shown in $Atg7$-deficient hepatocytes (Figure S11C). Electron microscopic analysis showed that the number of aggregate structures and aberrant concentric membranous structures that were typical in $Atg7$-deficient hepatocytes (Komatsu et al., 2005) were markedly reduced, whereas smooth endoplasmic reticulum and peroxisomes were still abundantly observed in DKO hepatocytes (Figure 4C).

Loss of p62 Suppresses Inclusion Formation in Autophagy-Deficient Neurons

We also examined the roles of p62 in inclusion formation in autophagy-deficient neurons. As shown in Figure S8, while no ubiquitin-positive inclusions were detected in the brains of wild-type and $p62$-knockout mice, ubiquitin-positive inclusions of various sizes were recognized immunohistochemically in several regions of the $Atg7^{F/F}$: Nes brain. Such inclusions were hardly detected in the $Atg7^{F/F}$:Nes:$p62^{-/-}$ (DKO) neurons (Figures 4D and S8). Unlike autophagy-deficient livers, it was difficult to convincingly detect by immunoblot analyses any differences in the amount of insoluble polyubiquitinated protein between $Atg7$- and $Atg7/p62$-DKO brain (Figures 4E and S10B). This discrepancy could be due to the relatively low amounts of insoluble ubiquitinated proteins in total brain lysates from $Atg7^{F/F}$:Nes mice, which were insufficient for the detection of the difference. Actually, the inclusions were observed in some restricted areas such as the hypothalamus and cerebral cortex, and they were hardly observed in glial cells (Hara et al., 2006; Komatsu et al., 2006). Previous electron microscopic analysis showed that the hypothalamic neurons in $Atg7^{F/F}$:Nes brain contained large inclusion bodies in the perikarya (Komatsu et al., 2006). Although such inclusions were hardly detected in the same region of DKO brain, we noticed the presence of several large neuritic structures with numer-

ous pleomorphic features of smooth endoplasmic reticulum (Figure 4F; c, e, and f). Similar alteration was also observed in the $Atg7^{F/F}$:Nes hypothalamus (Figure 4F, b and d), but not in the control (Figure 4F, a). In the cerebellar nuclei of both $Atg7^{F/F}$:Nes and DKO brains, which contained abundant round eosinophilic structures as evident in hematoxylin and eosin (H&E) stained sections (Figure 6C, bottom panel), myelinated axons were frequently enlarged and contained aberrant membranous structures and/or degenerated materials (Figures S12B–S12F), suggesting axonal degeneration in both $Atg7^{F/F}$: Nes and DKO neurons. Taken together, these results strongly suggest that the inclusion formation but not axonal degeneration is largely dependent on the presence of p62 in autophagy-deficient neurons.

Liver Injury in Autophagy-Deficient Mice Is Suppressed by Loss of p62

To examine whether abnormalities in autophagy-deficient liver are partly caused by the accumulation of p62, we examined the phenotypes of $Atg7^{F/F}$:Mx1:$p62^{-/-}$ mice. Surprisingly, simultaneous loss of $Atg7$ and $p62$ in the liver significantly suppressed the deleterious phenotypes caused by ablation of autophagy (Figures 5A and 5B). Indeed, histological analysis showed hepatocytic hypertrophy in $Atg7$-deficient liver and its suppression in DKO liver. Accordingly, the hepatic lobular structure was considerably better recognized in DKO than in $Atg7$-deficient liver (Figure 5C). While serum levels of aspartate aminotransferase (AST), alanine aminotransferase (ALT), and alkaline phosphatase (ALP) were elevated in the DKO mice compared with the control mice, the levels were markedly lower than those in single $Atg7$-deficient mice (Figure 5D). Almost the same results were observed in $Atg7^{F/F}$: Alb:$p62^{-/-}$ mice, which exhibited impaired autophagy in hepatocytes at postnatal stage, without plpC injection (Figure S13), indicating that plpC injection itself does not affect phenotypes of $Atg7^{F/F}$:Mx1 or $Atg7^{F/F}$:Mx1:$p62^{-/-}$ mice. Taken together, these results indicate that excess accumulation of p62 is a major cause of the pathogenic changes seen in the liver of autophagy-deficient mice.

Ablation of p62 Leads to Neither Improvement nor Exacerbation of the Phenotypes in Autophagy-Deficient Neurons

Further, to investigate whether defects in autophagy-deficient brain are also attributed to accumulation of p62 in neurons, we examined the phenotypes of $Atg7^{F/F}$: Nes:$p62^{-/-}$ mice. In contrast to the recovery of liver injury in $Atg7^{F/F}$:Mx1 mice by simultaneous loss of $p62$, ablation of $p62$ did not rescue behavioral abnormalities such as tremor and abnormal limb clasping recognized in $Atg7^{F/F}$: Nes mice (data not shown). Furthermore, histological

(E) Appearance of p62- and ubiquitin-positive inclusions in $Atg7$-deficient cerebral cortex during postnatal (P) development. $Atg7^{F/F}$:Nes mice were sacrificed at P2, 5, 11, and 28 days, and the brain sections were immunostained with anti-ubiquitin and p62 antibodies. Bottom panels show merged images. Bar, 20 μm.
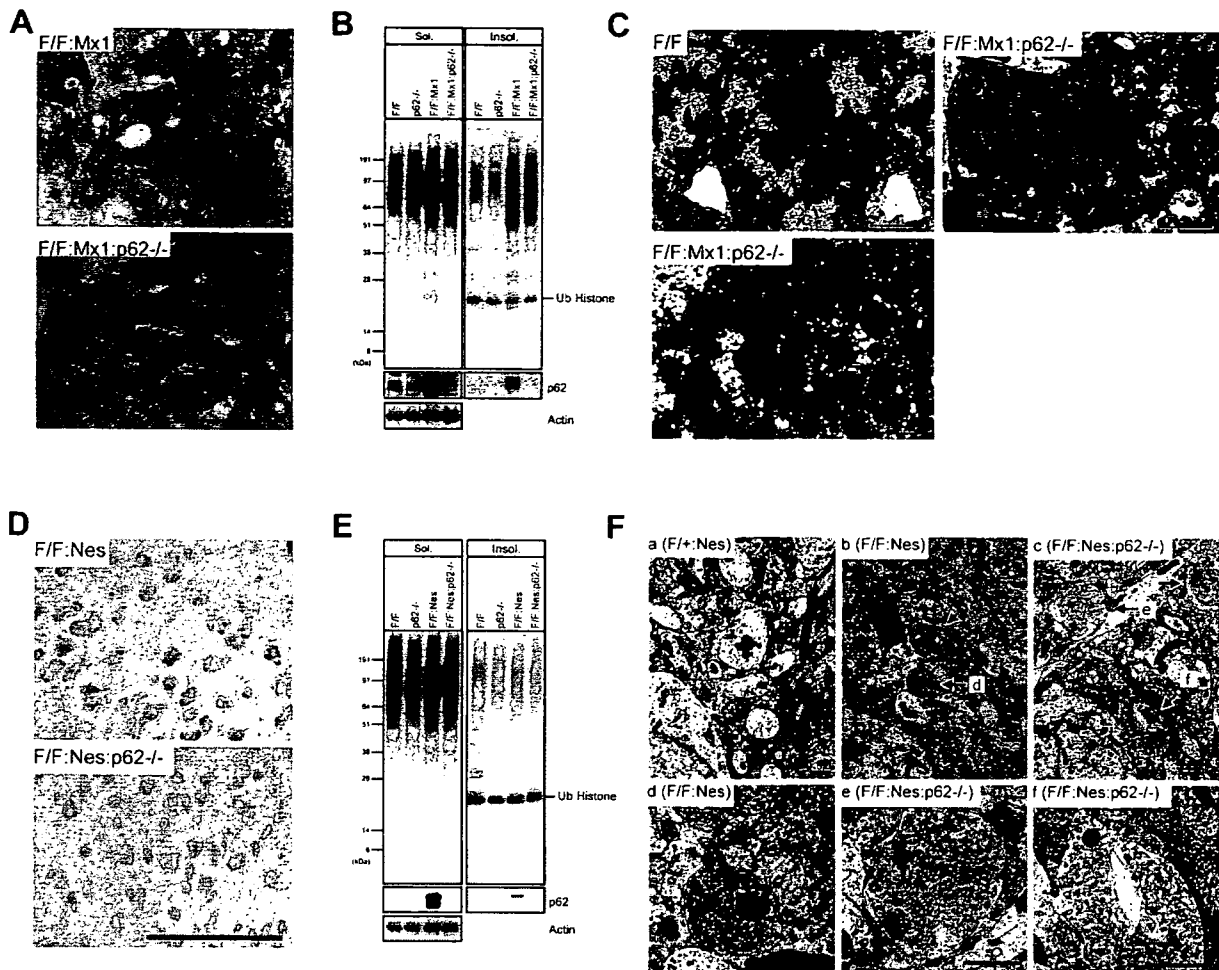
Figure 4. Indispensable Role of p62 in Inclusion Formation in Autophagy-Deficient Cells

(A) Immunohistochemical analysis of ubiquitin inclusions in Atg7- and Atg7/p62-deficient liver. Liver sections from $Atg7^{F/F}$:Mx1 and $Atg7^{F/F}$: Mx1:$p62^{-/-}$ mice at 14-day post-pIpC injection were immunostained with anti-ubiquitin antibody. Bar, 100 μm.

(B) Immunoblotting analysis of Atg7- and Atg7/p62-deficient livers. Liver homogenates from mice of the indicated genotype at 28-day post-pIpC injection were separated into detergent-soluble and insoluble fractions as shown in Figure 2. Each fraction was subjected to SDS-PAGE and analyzed by immunoblotting with indicated antibodies. Data shown are representative of three separate experiments.

(C) Electron micrographs of control and Atg7/p62-deficient liver. Note that the glycogen area (G), easily observed in control hepatocytes, is markedly reduced in Atg7/p62-deficient hepatocytes. The boxed region in the top right panel is further magnified in the bottom left panel. Asterisks indicate regions filled with smooth endoplasmic reticulum. Arrows indicate peroxisomes. Bars, 10 μm (left and right top panels) and 1 μm (left bottom panel).

(D) Immunohistochemical analysis of Atg7- and Atg7/p62-deficient brains. The presence of ubiquitin-positive particles was examined immunohisto-chemically in the hypothalamic regions of $Atg7^{F/F}$:Nes and $Atg7^{F/F}$:Nes:$p62^{-/-}$ mice. Bar, 100 μm.

(E) Immunoblotting analysis of Atg7- and Atg7/p62-deficient brains. Brain homogenates from mice of the indicated genotypes at 8 weeks of age were analyzed by immunoblotting as shown in (B). Data shown are representative of three separate experiments.

(F) Electron micrographs of the hypothalamus of mice of the indicated genotype. Note that several electron-lucent neuritic structures are detected in the control neuropil (a), which are only rarely seen in the Atg7- (b) and Atg7/p62-deficient (c) tissues. Instead, the latter tissues contain large neurites filled with pleomorphic features of smooth endoplasmic reticulum. Arrows indicate abnormal neuritic structures, some of which are magnified in d, e, and f. Bars, 1 μm.

analyses clearly revealed the lack of Purkinje cells in the cerebellum (Figure 6C) and large pyramidal neurons in both the cerebral cortex (Figure 6A) and hippocampus (Figure 6B) of $Atg7^{F/F}$:Nes:$p62^{-/-}$ as well as $Atg7^{F/F}$:Nes mice. We also found a number of eosinophilic spheroids in H&E-stained sections in the cerebellar nuclei of $Atg7^{F/F}$: Nes:$p62^{-/-}$ mice, similar to $Atg7^{F/F}$:Nes mice (Figure 6C). A marked increase in the number of TUNEL (terminal deox-

ynucleotidyl transferase [TdT]-mediated dUTP-biotin nick end labeling)-positive cells, which were noted in both $Atg7^{F/F}$:Nes cerebral cortices and granular cell layers of the cerebellum at P28, tended to decrease in similar regions of $Atg7^{F/F}$:Nes:$p62^{-/-}$ mice (Figures 6D and 6E), albeit sta-tistically insignificant. Thus, these results indicate that abla-tion of p62 does not result in improvement or exacerbation of the phenotypes in autophagy-deficient neurons.
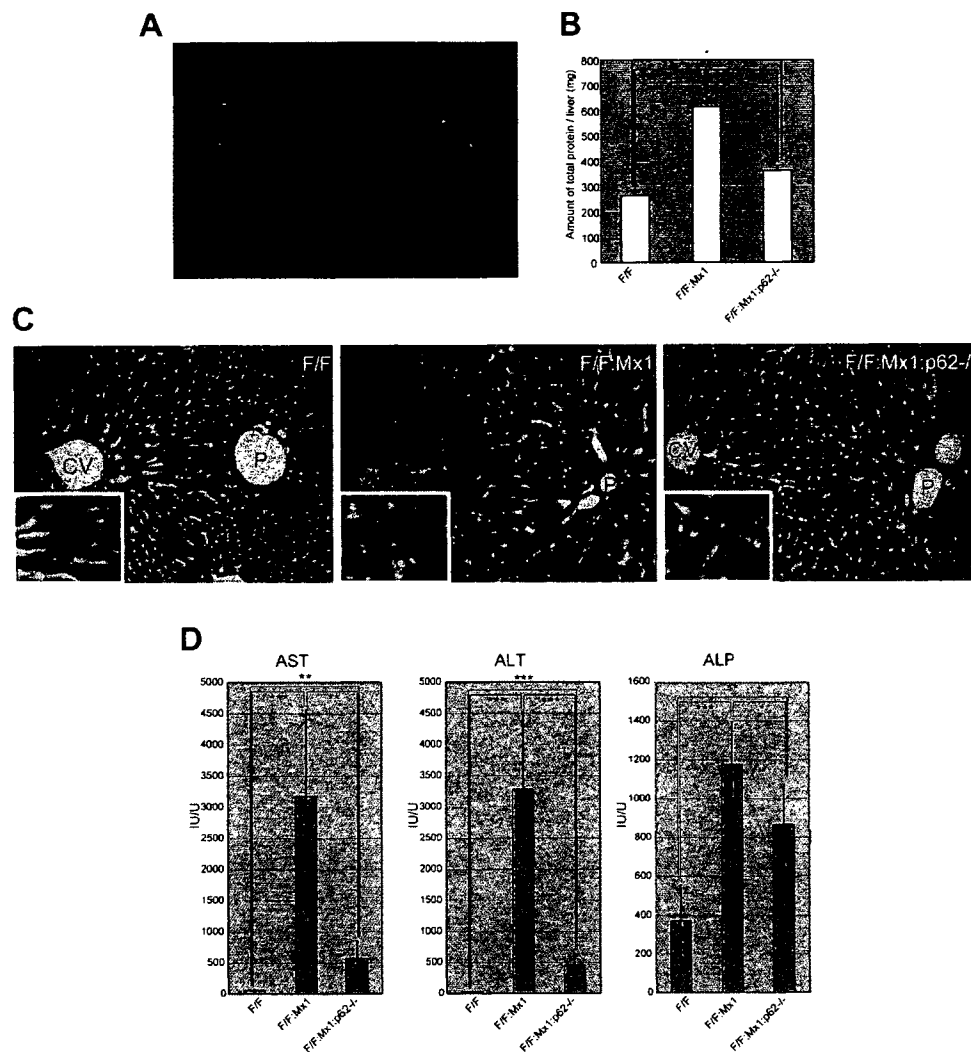
Figure 5. Suppression of Liver Dysfunction in Autophagy-Deficient Mice by Additional Loss of *p62*

(A) Gross anatomical views of representative livers from mice of the indicated genotype at 28-day post-pIpC injection.

(B) Amount of total liver protein. Livers from mice shown in (A) were dissected out, and amounts of total protein per liver were measured. Data are mean ± SD values of five mice in each group. *p < 0.05, **p < 0.01, and ***p < 0.001 (Student's t test).

(C) Typical histology of livers from mice of the indicated genotype. H&E staining of respective livers was conducted at 56-day post-pIpC injection. Higher magnification views are shown in insets. CV, central vein; P, portal vein. Bar, 100 μm.

(D) Liver function tests of mice shown in (A). Serum levels of AST, ALT, and ALP were measured. Data represent mean ± SD values of seven mice in each group. *p < 0.05, **p < 0.01, and ***p < 0.001.

Aberrant Accumulation of p62 Induces Detoxifying Enzymes in Livers but Not in Brains

Our data clearly showed that loss of *p62* suppresses liver dysfunction but not neurodegeneration in autophagy-deficient mice. How does p62 function differently in autophagy-deficient liver and brain? To elucidate the underlying mechanism for the difference, we examined gene-expression profiles in autophagy-deficient mice by microarray analyses and found that detoxifying enzymes including glutathione S-transferase (GST) families, cytochrome P450 families, and NAD(P)H dehydrogenase quinone 1 (Nqo1) were highly expressed in the autophagy-deficient liver. However, none of these detoxifying enzymes was upregulated in the autophagy-deficient brain (Figure 7A). Moreover, such induction in the liver was suppressed almost completely by additional loss of *p62* (Figure 7A). As shown in Figure 2D, accumulation and insolubilization of both p62 and ubiquitinated proteins began at 4 days post-pIpC injection in *Atg7^{F/F}*:Mx1 liver. Furthermore, upregulation of detoxifying enzymes began at 8 days and reached a plateau at 12 days post-pIpC injection (Figure 7B). Meanwhile, significant leakage of ALT and AST, representing hepatocyte death, occurred at later time points (Figure 7C), suggesting that the increase of detoxifying enzymes was not a secondary effect of liver dysfunction.
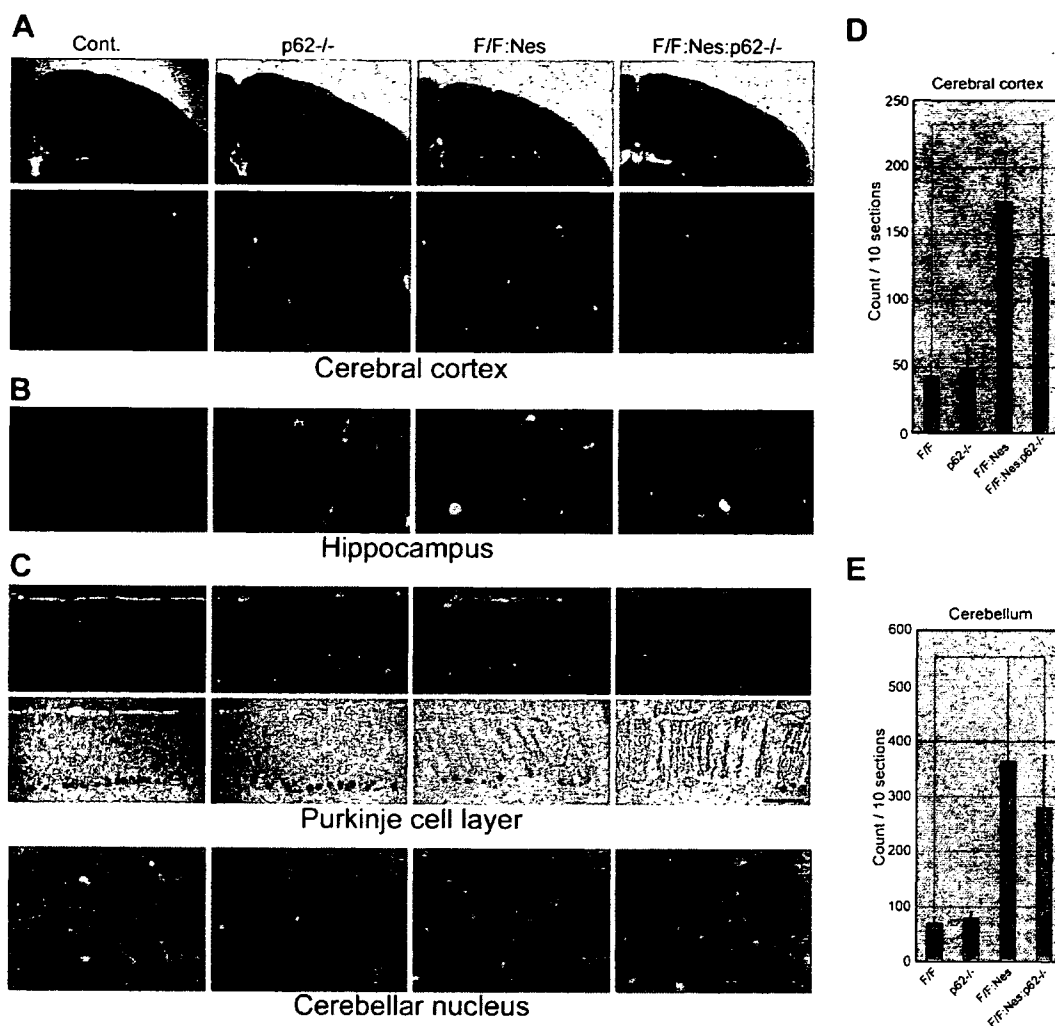
A Cont. p62-/- F/F:Nes F/F:Nes:p62-/- **D**

Cerebral cortex

B

Hippocampus

C **E**

Purkinje cell layer

Cerebellar nucleus

Figure 6. Ablation of p62 Leads to Neither Improvement nor Exacerbation of the Phenotypes in Autophagy-Deficient Neurons

(A and B) H&E staining of the cerebral cortex (A) and pyramidal cell layer of the hippocampus (B) in mice of the indicated genotype at 4 weeks of age. Top panels in (A) are magnified in bottom panels. Arrows in (A) point to large pyramidal neurons in the cerebral cortex.

(C) Histological analysis of the cerebellar cortex (top and middle panels) and cerebellar nucleus (bottom panel). Cryosections from 8-week-old mice were stained with H&E (top and bottom panels) or immunostained with Purkinje cell marker, calbindin (middle panels). Bars, 1 mm (A, top panel), 200 μm (C, bottom panel), 100 μm (A, bottom panel), (B and C, top and middle panels).

(D and E) Apoptotic cells in the cerebral cortex (D) and cerebellum (E) at 8 weeks of age of the indicated four genotypes. Bars represent the average number (±SD) of total TUNEL-positive cells in ten sections counted in three animals for each genotype. *p < 0.05.

A key question is how such enzymes are specifically induced in the autophagy-deficient liver. To this end, we examined the behavior of the transcriptional factor "Nrf2," which translocates to the nucleus in response to oxidative and electrophilic stresses to activate the transcription of various detoxifying enzymes including Gstm1 and Nqo1 (Tong et al., 2006). As shown in Figure 7D, the level of Nrf2 was markedly higher in the nuclear fraction from Atg7$^{F/F}$:Mx1 liver but very low in those from control and p62-knockout livers. Importantly, the translocation of Nrf2 into the nucleus in Atg7$^{F/F}$:Mx1 liver was almost completely suppressed by additional loss of p62, implying that autophagy-deficiency causes cellular stress in the liver, which negatively affects hepa-

tocyte function and concomitantly induces p62-dependent activation of Nrf2.

DISCUSSION

p62 Handles Formation of Cytoplasmic Inclusions

While there is ample evidence that dysfunction of the ubiquitin-proteasome system leads to the formation of ubiquitin-positive inclusions, which are the pathological hallmark of various neurodegenerative diseases (Goldberg, 2003), suppression of autophagy also leads to the formation of ubiquitin-positive inclusion (Hara et al., 2006; Komatsu et al., 2005, 2006). However, the molecular mechanism(s) involved in the formation of these inclusions is not clear to

date. In the present study, we found marked accumulation of p62 and ubiquitinated proteins and subsequent inclusion formation in Atg7-deficient mice (Figures 2 and 3). Intriguingly, p62 has been identified as a major component of ubiquitin-containing inclusions known as the "hepatocytic Mallory body" found in alcoholic hepatitis and steatohepatitis (Stumptner et al., 2002). Similar inclusions have been also recognized frequently in proteinaceous aggregates in the remnant neurons in various neurodegenerative disorders such as Parkinson's disease and amyotrophic lateral sclerosis (Kuusisto et al., 2001; Nakano et al., 2004). In such diseases, it is plausible that the reduced autophagic activity may be associated with the generation of inclusion bodies.

Surprisingly, loss of p62 was associated with marked reduction of ubiquitin-positive inclusions, which were otherwise abundantly present in Atg7-deficient hepatocytes and neurons (Figure 4). Because ubiquitin-tagged proteins are sticky but do not exhibit aggregation-prone nature themselves, the high levels of p62 due to impaired autophagy might predispose to inclusion formation via the PB1 domain, which retains the ability of self oligomerization (Lamark et al., 2003). Indeed, overexpression of p62 forms inclusions, which is dependent on the presence of both PB1 and UBA domains (Bjorkoy et al., 2005). Since almost all inclusions in autophagy-deficient cells were positive for both ubiquitin and p62, it is possible that ubiquitinated proteins initially interact with p62, and subsequently the protein complex becomes inclusions in a p62-dependent manner. Although autophagy is involved in protection from several discrete diseases (Fortun et al., 2003; Kamimoto et al., 2006; Ravikumar et al., 2004), whether p62 is indeed essential for the formation of disease-related inclusions or not remains unknown at present. However, intriguingly, the formation of ubiquitin-positive aggregates induced by proteasome inhibition is greatly suppressed in p62-deficient cells (Wooten et al., 2006), suggesting that p62 is a general mediator of inclusion formation.

p62-Dependent Liver Impairment in Autophagy-Deficient Mice

Our present studies suggest that the pathological changes in Atg7-deficient liver are due, at least in part, to oxidative stress associated with proteinaceous aggregates formed by excess accumulation of p62 and ubiquitinated proteins. However, emerging evidence indicates that protein aggregates containing disease-related proteins (e.g., polyQ) can provide protection (Arrasate et al., 2004; Ross and Poirier, 2005; Sanchez et al., 2003). Similarly, aggregate formation mediated by p62 seems to be a protective mechanism in the presence of overexpression of polyQ (Bjorkoy et al., 2005). Therefore, p62 might play an important role in the surveillance of protein abnormalities by adaptively segregating ubiquitin-tagged toxic proteins as inclusions in cells. It is noteworthy that oligomer and protofibrillar intermediates, which are cytotoxic (Arrasate et al., 2004; Ross and Poirier, 2005; Sanchez et al., 2003), must form before

the formation of harmless aggregates and generate reactive oxygen species, which are the primary mediators of oxidative stress (Tabner et al., 2005). Because genetic ablation of autophagy in the liver causes exhaustive accumulation of both p62 and ubiquitinated proteins, the liver might show mixed symptoms related to the cytotoxic effects and protective reactions—i.e., continuous formation of both "harmful oligomer and protofibrillar intermediates" and "harmless aggregates" and induction of both "oxidative stress" and "detoxifying enzymes." According to this scenario, simultaneous loss of p62 under autophagy-deficient background might attenuate accumulation of unfavorable harmful oligomer and protofibrillar intermediates, which ultimately form harmless inclusion, leading to alleviation of liver injury.

In this context, we found that impairment of liver autophagy led to nuclear translocation of Nrf2 (Figure 7D), which is responsible for inducible transcription of various antioxidant and detoxifying enzymes, providing mechanistic insights into the upregulation of those enzymes in the autophagy-deficient liver. In the absence of stress, Nrf2 is constitutively degraded through the ubiquitin-proteasome pathway, since the binding partner Keap1 is a ubiquitin-protein ligase. Exposure to oxidative and electrophilic insults results in modification of Cys residues of Keap1, and leads to inactivation of Keap1. Stabilization of Nrf2 leads to its nuclear translocation to induce the transcription of detoxifying enzymes (Tong et al., 2006). Accordingly, we surmise that the autophagy-deficient liver may be filled with oxidative and/or other Nrf2-inducing stresses. More interestingly, simultaneous loss of p62 and Atg7 completely suppressed the translocation of Nrf2 (Figure 7D). These results strongly argue for accumulation of cellular stress in autophagy-deficient liver, the extent of which depends on the impairment of p62 turnover, and they shed light on the mechanism of p62 loss-associated attenuation of autophagy-deficiency-related liver injury.

On the other hand, leakage of hepatocytic enzymes into peripheral blood still occurred at a significantly high level in $Atg7^{F/F}$:Mx1:$p62^{-/-}$ compared with control mice (Figure 5D), implying other abnormalities apart from p62 accumulation in the DKO livers. In fact, in addition to accumulation of soluble ubiquitinated proteins, impairment of organelle turnover was not rescued by the additional defect of p62 (Figures 4B and 4C). Such abnormalities together with the excess accumulation of p62 might have irreversible cytotoxic effects in autophagy-deficient hepatocytes.

p62-Independent Neuronal Death in Autophagy-Deficient Mice

Unlike the liver, the survival of Atg7-deficient neurons is affected little when p62 is abolished, although p62 can form protein aggregates in neuronal cells as in hepatocytes. This paradoxical observation may underlie the difference in autophagic activity among cell-types or tissues. The constitutive autophagic activity in the brain is low compared
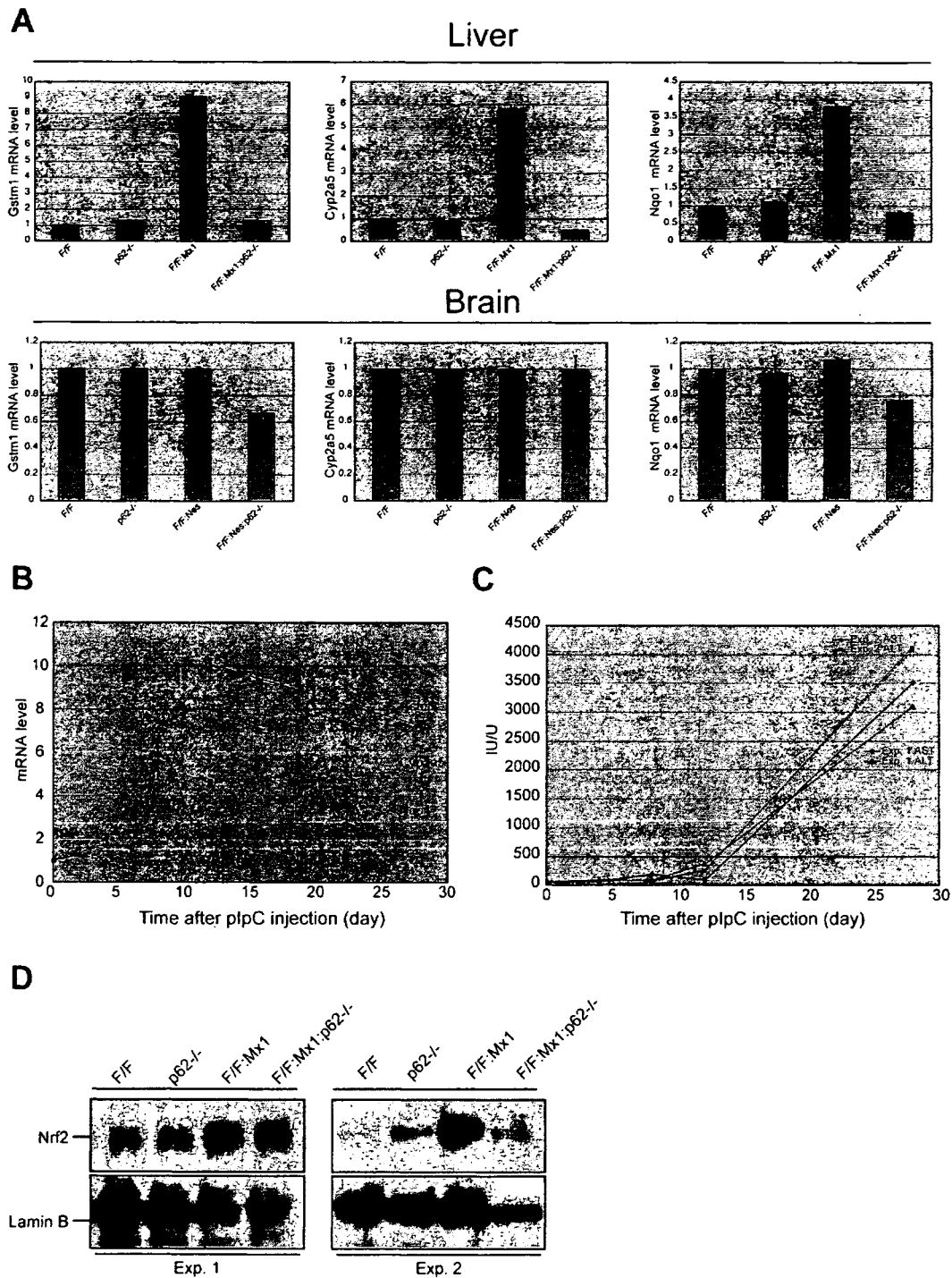
A

Liver

Brain

B

C

mRNA level

Time after pIpC injection (day)

IU/U

Time after pIpC injection (day)

D

Nrf2 —

Lamin B —

Exp. 1   Exp. 2

Figure 7. p62-Dependent Induction of Detoxifying Enzymes in Autophagy-Deficient Liver but Not in Brain

(A) Quantitative RT-PCR analyses of Gstm1, Cy2a5, and Nqo1 in mouse liver (top panels) and brain (bottom panels). Total RNAs were prepared from the livers of the indicated genotypes at 12 days post-pIpC injection and brains of the indicated genotypes at postnatal day 28. The values are normalized to the amount of mRNA in $Atg7^{F/F}$ liver and brain. The experiments were performed three times.

(B) Quantitation of mRNA levels of detoxifying enzymes in $Atg7^{F/F}$:Mx1 liver by RT-PCR. Total RNAs were prepared from $Atg7^{F/F}$:Mx1 mice livers at various time points post-pIpC injection, and then cDNA was synthesized from each RNA, followed by real-time PCR analyses. The values are normalized to the amount of each mRNA in $Atg7^{F/F}$:Mx1 liver at 0 days post-pIpC injection.

(C) Liver function tests of mice at various time points post-pIpC injection. Serum levels of AST and ALT were measured in $Atg7^{F/F}$:Mx1 mice. Data represent two independent mice.

with other tissues such as the liver (Mizushima et al., 2004). Accordingly, significant accumulation of ubiquitinated proteins was noted in *Atg7*-deficient brain, but their levels, especially insoluble ubiquitinated proteins, were lower than in *Atg7*-deficient liver (Figures 4E and S10B), and severe formation of the inclusion was found in restricted groups of neurons (Figures 4D and S8). Moreover, unlike in the liver, detoxifying enzymes did not increase in *Atg7*-deficient brain (Figure 7A), suggesting the low susceptibility of neurons to toxicity associated with aggregate formation. In fact, several ubiquitin-positive aggregates were recognized in *Atg7*-deficient brain regions in the presence of mild neuronal loss (Komatsu et al., 2006).

Why do autophagy-deficient mice develop neurodegeneration? Analyses of Purkinje cell-specific *Atg7*-knockout mice demonstrated that *Atg7*-deficient Purkinje cells initially causes cell-autonomous, progressive dystrophy (manifested by axonal swelling) and degeneration of the axon terminals followed by cell-autonomous Purkinje cell death and mouse behavioral deficits (Komatsu et al., 2007). The mutant Purkinje cells developed aberrant organelles in the swelling axons, suggesting the important role of autophagy in the regulation of local axonal membrane trafficking and turnover, and implicate impairment of axonal autophagy as a mechanism for axonopathy associated with neurodegeneration. Importantly, such axonopathy in *Atg7*-deficient Purkinje cells and hypothalamic neurons was still observed in *Atg7/p62*-DKO neurons (Figures 4F, 6C, and S12), indicating that the development of axonopathy in *Atg7*-deficient neurons is *p62* independent. Therefore, we hypothesize that the mechanism of neurodegeneration caused by autophagy deficiency might involve distinct pathogenic pathways, such as axonal dystrophy and degeneration.

EXPERIMENTAL PROCEDURES

Generation of Knockout Mice

Atg7$^{F/F}$:Mx1 mice (Komatsu et al., 2005) were bred with GFP-LC3 Tg mice (Mizushima et al., 2004) to generate *Atg7$^{F/F}$*:Mx1:GFP-LC3 mice. *p62$^{-/-}$* mice were bred with *Atg7$^{F/F}$*:Mx1, *Atg7$^{F/F}$*:Mx1:GFP-LC3, and *Atg7$^{F/F}$*:Nes mice (Komatsu et al., 2006) to generate *Atg7$^{F/F}$*:Mx1:*p62$^{-/-}$*, *Atg7$^{F/F}$*:Mx1:*p62$^{-/-}$*:GFP-LC3, and *Atg7$^{F/F}$*:Nes:*p62$^{-/-}$* mice, respectively. With regard to deletion of *Atg7* from the liver, Cre expression in the liver was induced by intraperitoneal injection of pIpC (Sigma Chemical Co., St. Louis, MO) (Komatsu et al., 2005). Mice were housed in specific-pathogen-free facilities, and the experimental protocol was approved by the Ethics Review Committee for Animal Experimentation of Tokyo Metropolitan Institute of Medical Science. Other mice strains shown in Supplemental Data are described in Supplemental Experimental Procedures.

Immunological Analysis

Livers and brains were homogenized in 0.25 M sucrose, 10 mM 2-[4-(2-hydroxyethyl)-1-piperazinyl]ethanesulfonic acid [HEPES], pH 7.4, and 1 mM dithiothreitol (DTT). The resultant homogenates were fractionated into 0.5% Tx-100 soluble and insoluble fractions. Immunoprecipitation and immunoblot analyses were conducted as described pre-

viously (Komatsu et al., 2004). Nuclear fraction from the liver was prepared according to the method of Blobel and Potter (Blobel and Potter, 1966). The antibodies for p62, Atg7, and LC3 were described previously (Ishii et al., 1996; Komatsu et al., 2005). The antibodies for GFP (Medical and Biological Laboratories [MBL] Co., Nagoya, Japan), ubiquitin (FK2: MBL), Nrf2 (H-300: Santa Cruz Biotechnology, Inc., Santa Cruz, CA), LDH (ab2101: abcam, Inc., Cambridge, MA), actin (MAB1501R: Chemicon International, Inc., Temecula, CA) and Lamin B (M-20: Santa Cruz Biotechnology, Inc.) were purchased.

Pull-Down Assay

Recombinant GST, GST-LC3, and GST-p62 were produced in *Escherichia coli*, and recombinant proteins were purified by chromatography on glutathione-Sepharose 4B (Amersham Biosciences, Arlington Heights, IL). The GST-p62 cleaved the GST tag by precision protease (Amersham Biosciences). Purified p62 and GST or GST-LC3 were mixed in TNE buffer (Komatsu et al., 2004) for 3 hr at 4°C and then precipitated with glutathione-Sepharose. The mixtures were washed five times with ice-cold TNE. The bound proteins were analyzed by SDS-PAGE followed by Coomassie brilliant blue (CBB) staining.

Quantitative RT–PCR

cDNA was synthesized from 1 μg of total RNA using the Transcriptor First Strand cDNA Synthesis Kit (Roche Applied Science), and quantitative PCR was performed using LightCycler 480 Probes Masterin (Roche Applied Science) in a LightCycler 480 (Roche Applied Science). Signals were normalized to β-glucronidase (GUS). Primer sequences are described in Supplemental Experimental Procedures.

Immunofluorescence Microscopy of Cultured Hepatocytes

Hepatocytes grown on glass coverslips were immunostained with anti-p62 or ubiquitin (DakoCytomation, Glostrup, Denmark) antibody as described previously (Komatsu et al., 2005). The coverslips were mounted and viewed with a laser-scanning confocal microscope (FV1000, Olympus) or conventional epifluorescent microscope.

Histological Examination

Methods for tissue fixation and subsequent procedures, including H&E staining, immunohistochemistry, conventional electron microscopy, immunoelectron microscopy, and TUNEL staining were described previously (Komatsu et al., 2005, 2006). Antibodies used for immunohistochemistry and immunoelectron microscopy were as follows: rabbit polyclonal antibodies against LC3 (Komatsu et al., 2005), p62 (Ishii et al., 1996), and GFP (Abcam), and mouse monoclonal antibodies against ubiquitin (FK2 and 1B3: MBL).

Statistical Analysis

Data were analyzed by two-tailed Student's t test. For all graphs, data are represented as mean ± SD.

Supplemental Data

Supplemental Data include 13 figures, 1 table, Supplemental Experimental Procedures, and Supplemental References and can be found with this article online at http://www.cell.com/cgi/content/full/131/6/1149/DC1/.

(D) The level of Nrf2 in liver nuclear fraction. Nuclear fractions were prepared from liver of the indicated genotypes at 12 days post-pIpC injection, subjected to SDS-PAGE, and analyzed by immunoblotting with antibodies against Nrf2 and Lamin B (as a control). Data represent two independent mice.

REFERENCES

Arrasate, M., Mitra, S., Schweitzer, E.S., Segal, M.R., and Finkbeiner, S. (2004). Inclusion body formation reduces levels of mutant huntingtin and the risk of neuronal death. Nature 431, 805–810.

Bjorkoy, G., Lamark, T., Brech, A., Outzen, H., Perander, M., Overvatn, A., Stenmark, H., and Johansen, T. (2005). p62/SQSTM1 forms protein aggregates degraded by autophagy and has a protective effect on huntingtin-induced cell death. J. Cell Biol. 171, 603–614.

Blobel, G., and Potter, V.R. (1966). Nuclei from rat liver: isolation method that combines purity with high yield. Science 154, 1662–1665.

Elmore, S.P., Qian, T., Grissom, S.F., and Lemasters, J.J. (2001). The mitochondrial permeability transition initiates autophagy in rat hepatocytes. FASEB J. 15, 2286–2287.

Fortun, J., Dunn, W.A., Jr., Joy, S., Li, J., and Notterpek, L. (2003). Emerging role for autophagy in the removal of aggresomes in Schwann cells. J. Neurosci. 23, 10672–10680.

Goldberg, A.L. (2003). Protein degradation and protection against misfolded or damaged proteins. Nature 426, 895–899.

Hara, T., Nakamura, K., Matsui, M., Yamamoto, A., Nakahara, Y., Suzuki-Migishima, R., Yokoyama, M., Mishima, K., Saito, I., Okano, H., and Mizushima, N. (2006). Suppression of basal autophagy in neural cells causes neurodegenerative disease in mice. Nature 441, 885–889.

Ichimura, Y., Kirisako, T., Takao, T., Satomi, Y., Shimonishi, Y., Ishihara, N., Mizushima, N., Tanida, I., Kominami, E., Ohsumi, M., et al. (2000). A ubiquitin-like system mediates protein lipidation. Nature 408, 488–492.

Ishii, T., Yanagawa, T., Kawane, T., Yuki, K., Seita, J., Yoshida, H., and Bannai, S. (1996). Murine peritoneal macrophages induce a novel 60-kDa protein with structural similarity to a tyrosine kinase p56lck-associated protein in response to oxidative stress. Biochem. Biophys. Res. Commun. 226, 456–460.

Iwata, J., Ezaki, J., Komatsu, M., Yokota, S., Ueno, T., Tanida, I., Chiba, T., Tanaka, K., and Kominami, E. (2006). Excess peroxisomes are degraded by autophagic machinery in mammals. J. Biol. Chem. 281, 4035–4041.

Kabeya, Y., Mizushima, N., Ueno, T., Yamamoto, A., Kirisako, T., Noda, T., Kominami, E., Ohsumi, Y., and Yoshimori, T. (2000). LC3, a mammalian homologue of yeast Apg8p, is localized in autophagosome membranes after processing. EMBO J. 19, 5720–5728.

Kamimoto, T., Shoji, S., Hidvegi, T., Mizushima, N., Umebayashi, K., Perlmutter, D.H., and Yoshimori, T. (2006). Intracellular inclusions containing mutant alpha1-antitrypsin Z are propagated in the absence of autophagic activity. J. Biol. Chem. 281, 4467–4476.

Komatsu, M., Chiba, T., Tatsumi, K., Iemura, S., Tanida, I., Okazaki, N., Ueno, T., Kominami, E., Natsume, T., and Tanaka, K. (2004). A novel protein-conjugating system for Ufm1, a ubiquitin-fold modifier. EMBO J. 23, 1977–1986.

Komatsu, M., Waguri, S., Ueno, T., Iwata, J., Murata, S., Tanida, I., Ezaki, J., Mizushima, N., Ohsumi, Y., Uchiyama, Y., et al. (2005). Impairment of starvation-induced and constitutive autophagy in Atg7-deficient mice. J. Cell Biol. 169, 425–434.

Komatsu, M., Waguri, S., Chiba, T., Murata, S., Iwata, J., Tanida, I., Ueno, T., Koike, M., Uchiyama, Y., Kominami, E., and Tanaka, K. (2006). Loss of autophagy in the central nervous system causes neurodegeneration in mice. Nature 441, 880–884.

Komatsu, M., Wang, Q.J., Holstein, G.R., Friedrich, V.L., Iwata, J.I., Kominami, E., Chait, B.T., Tanaka, K., and Yue, Z. (2007). Essential role for autophagy protein Atg7 in the maintenance of axonal homeostasis and the prevention of axonal degeneration. Proc. Natl. Acad. Sci. USA 104, 14489–14494.

Kuma, A., Hatano, M., Matsui, M., Yamamoto, A., Nakaya, H., Yoshimori, T., Ohsumi, Y., Tokuhisa, T., and Mizushima, N. (2004). The role of autophagy during the early neonatal starvation period. Nature 432, 1032–1036.

Kuusisto, E., Salminen, A., and Alafuzoff, I. (2001). Ubiquitin-binding protein p62 is present in neuronal and glial inclusions in human tauopathies and synucleinopathies. Neuroreport 12, 2085–2090.

Lamark, T., Perander, M., Outzen, H., Kristiansen, K., Overvatn, A., Michaelsen, E., Bjorkoy, G., and Johansen, T. (2003). Interaction codes within the family of mammalian Phox and Bem1p domain-containing proteins. J. Biol. Chem. 278, 34568–34581.

Levine, B., and Klionsky, D.J. (2004). Development by self-digestion: molecular mechanisms and biological functions of autophagy. Dev. Cell 6, 463–477.

Mizushima, N., Yamamoto, A., Hatano, M., Kobayashi, Y., Kabeya, Y., Suzuki, K., Tokuhisa, T., Ohsumi, Y., and Yoshimori, T. (2001). Dissection of autophagosome formation using Apg5-deficient mouse embryonic stem cells. J. Cell Biol. 152, 657–668.

Mizushima, N., Yamamoto, A., Matsui, M., Yoshimori, T., and Ohsumi, Y. (2004). In vivo analysis of autophagy in response to nutrient starvation using transgenic mice expressing a fluorescent autophagosome marker. Mol. Biol. Cell 15, 1101–1111.

Moscat, J., Diaz-Meco, M.T., Albert, A., and Campuzano, S. (2006). Cell signaling and function organized by PB1 domain interactions. Mol. Cell 23, 631–640.

Nakano, T., Nakaso, K., Nakashima, K., and Ohama, E. (2004). Expression of ubiquitin-binding protein p62 in ubiquitin-immunoreactive intraneuronal inclusions in amyotrophic lateral sclerosis with dementia: analysis of five autopsy cases with broad clinicopathological spectrum. Acta Neuropathol. (Berl.) 107, 359–364.

Ohsumi, Y. (2001). Molecular dissection of autophagy: two ubiquitin-like systems. Nat. Rev. Mol. Cell Biol. 2, 211–216.

Ravikumar, B., Vacher, C., Berger, Z., Davies, J.E., Luo, S., Oroz, L.G., Scaravilli, F., Easton, D.F., Duden, R., O'Kane, C.J., and Rubinsztein, D.C. (2004). Inhibition of mTOR induces autophagy and reduces toxicity of polyglutamine expansions in fly and mouse models of Huntington disease. Nat. Genet. 36, 585–595.

Rodriguez, A., Duran, A., Selloum, M., Champy, M.F., Diez-Guerra, F.J., Flores, J.M., Serrano, M., Auwerx, J., Diaz-Meco, M.T., and Moscat, J. (2006). Mature-onset obesity and insulin resistance in mice deficient in the signaling adapter p62. Cell Metab. 3, 211–222.

Ross, C.A., and Poirier, M.A. (2005). Opinion: What is the role of protein aggregation in neurodegeneration? Nat. Rev. Mol. Cell Biol. 6, 891–898.

Sanchez, P., De Carcer, G., Sandoval, I.V., Moscat, J., and Diaz-Meco, M.T. (1998). Localization of atypical protein kinase C isoforms into lysosome-targeted endosomes through interaction with p62. Mol. Cell. Biol. 18, 3069–3080.

Sanchez, I., Mahlke, C., and Yuan, J. (2003). Pivotal role of oligomerization in expanded polyglutamine neurodegenerative disorders. Nature 421, 373–379.

Stumptner, C., Fuchsbichler, A., Heid, H., Zatloukal, K., and Denk, H. (2002). Mallory body-a disease-associated type of sequestosome. Hepatology 35, 1053–1062.

Tabner, B.J., El-Agnaf, O.M., German, M.J., Fullwood, N.J., and Allsop, D. (2005). Protein aggregation, metals and oxidative stress in neurodegenerative diseases. Biochem. Soc. Trans. 33, 1082–1086.

Tong, K.I., Kobayashi, A., Katsuoka, F., and Yamamoto, M. (2006). Two-site substrate recognition model for the Keap1-Nrf2 system: a hinge and latch mechanism. Biol. Chem. *387*, 1311–1320.

Tsukada, M., and Ohsumi, Y. (1993). Isolation and characterization of autophagy-defective mutants of Saccharomyces cerevisiae. FEBS Lett. *333*, 169–174.

Wang, Q.J., Ding, Y., Kohtz, D.S., Mizushima, N., Cristea, I.M., Rout, M.P., Chait, B.T., Zhong, Y., Heintz, N., and Yue, Z. (2006). Induction of autophagy in axonal dystrophy and degeneration. J. Neurosci. *26*, 8057–8068.

Wooten, M.W., Hu, X., Babu, J.R., Seibenhener, M.L., Geetha, T., Paine, M.G., and Wooten, M.C. (2006). Signaling, polyubiquitination, trafficking, and inclusions: Sequestosome 1/p62's role in neurodegenerative disease. J. Biomed. Biotechnol. *2006*, 62079.